DEVELOPING EMISSION FACTORS OF FUGITIVE PARTICULATE MATTER EMISSIONS FOR CONSTRUCTION SITES IN THE MIDDLE EAST

A Thesis

by

HALA ABDELRAHMAN MEDANI HASSAN

Submitted to the Office of Graduate and Professional Studies of
Texas A&M University
in partial fulfillment of the requirements for the degree of

MASTER OF SCIENCE

Chair of Committee,	Konstantinos E. Kakosimos
Committee Members,	Mohamed Nounou
	Qi Ying
Head of Department,	M. Nazmul Karim

May 2015

Major Subject: Chemical Engineering

ABSTRACT

A major source of airborne pollution in the arid Middle East countries is the fugitive particulate matter (PM), a frequent product of wind erosion. The meteorological conditions and topography of this region makes it highly susceptible to wind-blown particles which raise many air quality concerns. Important tools for estimating the dispersion and deposition of dust particles, which also help in designing dust control procedures, are Air Quality Models (AQM). The cornerstone of every AQM system is an emission inventory, but these are only available currently for the European and North American domains, calling for an immediate need to develop similar knowledge for MEA.

The increasing level of urbanization in Middle East countries has thrown the light on the airborne pollution caused by construction and earth work activities. The main scope of the present study is to develop fugitive particulate matter emission factors for construction sites in MEA and to evaluate the accuracy of the existing emission factors to apply for Middle Eastern hot and arid conditions. An experimental campaign along with dispersion modeling using the Fugitive Dust Model (FDM) were implemented in a construction site to examine the relation between the meteorological variables, concentrations and emission rates to understand the behavior of the fugitive dust emissions for MEA. The time period of this work was chosen while the construction site was at rest, where the only particles source was wind erosion of the loose soil. A data analysis was done, using the modeling results, to identify the effect of each

meteorological variable (i.e. wind direction, wind speed, stability, .etc.) and its relation to emissions concentrations and rates. Considering the wind-speed dependence of the source emission rate, a power law function was obtained for the calculation of the emission rates. This function was used to re-run the FDM model and the results were evaluated compared to the on-site measured concentrations and to the emission factors reported in USEPA's AP-42 (the related emission rates in this emission inventory have been developed mainly for open coal-mines). Surprisingly, our study showed that a very good agreement between the AP-42 emission factors and our calculations can be obtained if the former are slightly modified. The emission factors developed in this study have been confirmed and can be applied for the impact assessment of similar sources in Middle East and other dry-arid locations.

DEDICATION

"In The Name of Allah, The Most Beneficent, The Most Merciful"

I dedicate this thesis to my loving parents, Abdelrahman & Fatin, who have always loved me unconditionally and taught me to work hard for the things that I aspire to achieve, and to my beautiful sister, Sara, and brother, Ahmed, for their endless love and support.

A special dedication goes to my husband Nader, my better half, whom without, I'm never complete. "Thank you my dear for believing in me, and for all the patience, love and support you showered me with throughout this journey".

I also dedicate this thesis to my best friend, Rehaid, a person who has always been by my side and inspired me to pursue what I believe in.

Finally, I dedicate this thesis to my beloved country, Sudan, and I pray that it stays strong and fights for a better future and ultimate peace.

ACKNOWLEDGEMENTS

I would like to thank my committee chair, Dr. Konstantinos E. Kakosimos, for his guidance and support throughout the course of this research, and the same is extended to my committee members, Dr. Mohamed Nounou and Dr. Qi Ying.

A special thank you goes to Dr. Vasiliki Tsiouri, for her support with this research work and for sharing her knowledge on the subject.

I also would like to extend my gratitude to Qatar National Research Fund (a member of the Qatar Foundation) which made this work possible through the NPRP award [NPRP 7 - 649 - 2 - 241]., and to Qatar Foundation's Capital Projects Department, for their contribution in facilitating the experimental campaign conducted within the QF Education City premises.

Finally, thanks to my colleagues and the department faculty and staff for making my time at Texas A&M University a great experience.

Parts of this work were published in a paper for the participation in ICAPC 2015: XIII International Conference on Air Pollution and Control organized by World Academy of Science, Engineering and Technology (www.waste.org).

NOMENCLATURE

AQM	Air Quality Model
AQMEII	Air Quality Model Evaluation International Initiative
E, E`	Emission Rate
EEA	European Environment Agency
FDM	Fugitive Dust Model
K	Eddy Diffusivity
NPI	National Pollutant Inventory
P_i	Erosion Potential
PM	Particulate Matter
Q_o	Proportionality Constant
Tg	Teragram
TSP	Total Suspended Particles
u	Wind Speed
u*	Friction Velocity
UNEP	United Nations Environment Programme
USEPA	United States Environmental Protection Agency
w	Wind speed dependence factor
WHO	World Health Organization
χ	Pollutant Concentration (g/m^3)
σ_y, σ_z	Standard Deviation of Concentration in y and z directions

TABLE OF CONTENTS

Page

LIST OF FIGURES

Page

LIST OF TABLES

Page

CHAPTER I

INTRODUCTION

I.1 Introduction

The Middle East Area (MEA) is highly affected by air pollution induced by anthropogenic and natural sources. A major source of airborne pollution in the arid Middle East countries is the fugitive particulate matter (PM) [1], a frequent product of wind erosion. The meteorological conditions and topography of this region makes it highly susceptible to wind-blown particles which raise many air quality concerns. Many hazardous contaminants, such as minerals are associated with and transported by dust, and have severe impacts on human health and environment [2-5]. There is substantial evidence that airborne PM contributes to haze, acid rain, global climate change, asthma and other respiratory ailments, cardiopulmonary disease, and decreased life expectancy. The severity of PM effects on human health depends mainly on the concentration levels and length of the exposure [6]. Several studies, during the last decade, have reported adverse health effects of PM related to both long and short term exposure [6, 7].

Important tools for estimating the dispersion and deposition of dust particles, which also help in designing dust control procedures, are Air Quality Models (AQM) [8]. The United States Environmental Protection Agency (USEPA) has approved a wide range of atmospheric dispersion models [9]. These Models can predict concentrations of various pollutants on both local and regional scales; however, most of the well validated models have limitations when estimating concentrations from fugitive dust sources [10].

One of the most commonly used models to compute concentration and deposition impacts of fugitive dust sources is the “Fugitive Dust Model” (FDM), a Computerized Gaussian air quality model developed by USEPA [11].

The base of each air quality management system (AQM) is an emission inventory; however, the currently available inventories are only for the European and North American domains [12], which alerts for the need to develop the same information for MEA. These inventories include fugitive particulate emissions caused by wind shear, material transfer processes or other mechanical processes such as agriculture, road traffic, construction and industrial activities. Particles generated by natural source, like windblown dust and sea salt, are also included in these inventories. Some recent studies threw the light on the shortage of emissions inventories for MEA [13], and the need to develop an understanding of the local physio-chemical characteristics and sources of PM.

The accuracy of an AQM depends on the accuracy of the input emission rates of the pollutants [14]. Emission rates can be estimated using data from air quality monitors or by using empirical emission factors developed by well-established environmental institutions such as USEPA or the European Environment Agency (EEA). In the work of Abdel-Wahab, where the impact of fugitive dust emissions from a cement plant was assessed [10], the dust mission rates from various sources (cement manufacturing activities, storage piles and equipment traffic) were estimated using the emission factors reported in the National Pollutant Inventory (NPI) manual [15]. The calculated emission rates along with meteorological and receptor data were entered into FDM model to

compute the dust emission concentrations. Model predictions were then validated by placing high-volume samplers at residential areas adjacent to a cement plant to collect TSP particles, and calculate the concentrations using the volume of the sample. The predicted and observed values were evaluated based on 24-h average concentrations. Although the FDM model showed an under-prediction of TSP concentrations, it proved to be adequate based on the performance evaluation performed using correlation and regression coefficients.

A recent study was conducted by Ono et al. [16] to quantify windblown dust at Mono Lake, California. This work presents a different method following Owens Lake Dust Identification Program (Dust ID). This method benefits from the theoretically & experimentally evidenced proportionality between the vertical PM_{10} flux and the horizontal sand flux. The methodology in this study was based on measuring 1-h horizontal sand fluxes and relates them to the 1-h PM_{10} concentrations, and the "AERMOD" dispersion model was used to back-calculate seasonal K-factors (i.e. the ratio of vertical PM10 flux to horizontal sand flux). Next, the seasonal K-factors were used to re-calculate the 1-h PM_{10} emissions and compare them to the monitored PM_{10} concentrations. The results obtained in this study concluded that the wind erosion is not a simple function of wind speed, as assumed by the AP-42 wind-tunnel emission algorithms, and that the estimation of PM_{10} concentrations using the sand flux measurements and K-factors provides better modeling results since they account for the change in surface conditions.

In a more recent study by Sanderson [17], dust emissions from smelter slag were calculated using an experimental-based approach. A physical difference was introduced in this study; that is fugitive dust entrained from smelter slag doesn't depend on a defined threshold friction velocity unlike that of the development of saltation cloud. The mass emission rate was calculated using the control volume method and data from wind experiment. Vertical dust flux was also calculated using finite difference approximation and gave a good agreement with the predicted emission rate. The obtained values were validated though direct field measurements using non-isokinetic TSI DustTrack aerosol monitors, which confirmed a good agreement between the measured and predicted emissions.

In another recent work by Kinsey et al. [18], time-integrated and continuous exposure profiling were used to evaluate the emission factors of PM_{10} and $PM_{2.5}$ (i.e. particulate matter ≤10 and 2.5 μm in classical aerodynamic diameter, respectively) for mud/dirt carryout from a major construction site in metropolitan Kansas City, MO. The evaluation showed that although the emission factor for PM_{10} was in agreement with the reported in USEPA's AP-42, the $PM_{2.5}$ was way lower.

In the present study, an experimental campaign along with the dispersion modeling are used to correlate meteorological variables, concentrations and emission rates to understand the behavior of the fugitive dust emissions in MEA. The focus in this work is on construction sites at rest, giving the fact that the fugitive emissions from this source are poorly known for the Middle East [1]. An experimental campaign was implemented in a construction site and a background location to get the PM contribution

from both. FDM dispersion model was used next to estimate the source-receptor relation. The ultimate goal is to examine the fugitive PM releases from construction sector in Middle East area to obtain the missing information in understanding the behavior of fugitive PM sources and their impact of public health.

I.2 Scope of Thesis

The scope of the present study is to develop fugitive particulate matter emission factors for construction sites in MEA and to evaluate the accuracy of the existing emission factors, reported in USEPA's AP-42, to apply for Middle Eastern hot and arid conditions.

CHAPTER II

PM EMISSIONS IN MIDDLE EAST AREA

II.1 Fugitive Particulate Matter Sources and Health Impact

Middle East Area (MEA) is experiencing a rapid rate of urbanization, industrialization and construction, which raises many health concerns related to the increasing exposure to airborne particulate matter (PM) (Figure 1) [1]. The MEA has many significant sources of PM; that includes natural sources (sea salt, and wind-blown dust from the bare land/desert), construction sector (building, recycling and demolition) and road traffic (break, street surface and tire abrasion and dust).

Fugitive dust particles are particles that escape to the atmosphere in an unconfined flow when applying a mechanical force to a surface material, or entrained by air currents such as wind erosion [19], which results from two types of forces: "aerodynamic forces" that cause the removal of particles from the surface, and is determined by the "wind friction velocity", a measure of wind shear at the surface, and forces that resist particles removal such as "gravitational and inter-particle cohesion forces" [2]. Dust particles get entrained into the atmosphere when wind speed exceeds a critical value called the "threshold friction velocity" [14, 20]. The threshold friction velocity is the minimum velocity required to originate particle movement. The ability of particles to disperse and deposit depend on their shape and size [21], while other factors such as soil texture, moisture and chemical composition affect the quantity of emitted dust particles [16].

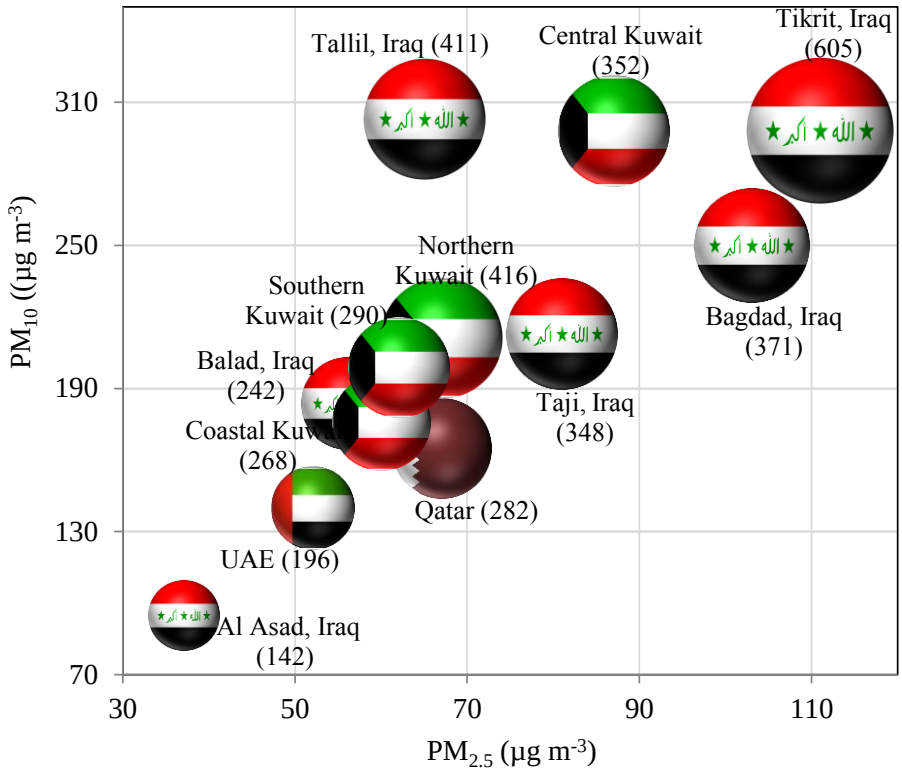

Figure 1 Bubble graph showing annual mean mass concentrations for TSP, PM_{10} and $PM_{2.5}$ in MEA countries. The size of the bubble corresponds to the TSP concentrations (value in parenthesis is in µg/m^3) [1]

Many epidemiological studies have linked the exposure to high levels of ambient PM with serious health effects, such as lung cancer and cardiovascular mortality, depending on the length of exposure [22, 23]. Cities in the Middle East, such as Damascus, Baghdad and Manama, experience high air pollution levels that break the WHO guidelines for PM_{10} and $PM_{2.5}$, according to the 2012 Yearbook of the UNEP Global Environmental Outlook. The Egyptian Environment Affairs Agency stated that air pollution in Cairo causes around 3,400 deaths, 15,000 cases of bronchitis, and 329,000 cases of respiratory infection every year [1]. A recent study by Gibson et al.

[24], concerning the deaths and medical visits attributable to environmental pollution in the United Arab Emirates, concluded that air pollution is the lead contributor to mortality with a percentage of ~7.3% of total deaths in 2008 in UAE.

II.1.1 Fugitive Dust from Construction Sites

The increasing level of urbanization in Middle East countries calls for an immediate investigation of the airborne hazards associated with construction and earth work activities. Many countries in the MEA, such as Qatar and UAE, experience continuous construction activities all year long. Qatar, for example, will spend US$160 billion on infrastructure in the coming years [25].The construction activities have been found to increase particle mass concentrations near the building sites. Although this increase is expected to be for short periods [26], it can cause serious respiratory health effects to people living or working nearby. Construction activities, such crushing, drilling, cutting and screening, will cause PM releases that escape to the air due to re-suspension and mechanical attrition between building materials [1].

Although construction sector is a major contributors to PM pollution, there are very few studies concerning PM releases from construction activities [27]. Therefore studies focused on PM pollution from construction activities are utmost important for the development of air quality policies to control PM at building sites.

II.1.3 Climate

The climate and meteorological conditions of an area, including temperature, wind speed, wind direction, humidity, atmospheric pressure and height of the mixing layer are major factors that affect the dispersion of particulate matter [28, 29].

MEA has a dry climate with high temperatures, dust storms, and limited rainfall [30]. MEA is a part of the arid belt that extends from the Sahara desert in Africa to Western Asia, except the humid and rainy territories in the coastal highlands of Lebanon and in the Iraqi highlands. In general, aridity prevails in the area and the climate is characterized by long summers (of six months, sometimes longer) and daily average temperatures above 35 ºC [1]. A brief summary of the climate in MEA countries is presented in (Table 1).

Table 1 Summary of the climate in MEA countries [1]

MEA Countries	Climate
Bahrain	Arid; very hot, humid summers; mild winters
Egypt	Hot desert, generally dry climate; hot summers; mild winters (November to April)
Iran	Mostly arid or semiarid; subtropical along Caspian coast
Iraq	Hot, dry climate; long, hot, dry summers; short, cool winters
Israel	Temperate; hot and dry in southern and eastern desert areas
Jordan	Mostly arid desert; rainy season in west (November to April)
Kuwait	Dry desert; intensely hot summers; short and cool winters
Lebanon	Dry desert; intensely hot summers; short and cool winters
Oman	Hot, arid climate; long and very hot summers; warm winters; precipitation is scarce
Palestine	Temperate, Mediterranean climate; rainy season (November to April)
Qatar	Hot desert climate; long summer (May to September); scarce rainfall; warm winters
Saudi Arabia	Dry desert with great temperature extremes
Syria	Mediterranean influenced climate; long, hot and mostly dry summers; mild, wet winters
UAE	Subtropical dry, hot desert climate; low annual rainfall
Yemen	Subtropical dry, hot desert climate; low annual rainfall; very high temperatures in summer

II.2 Emission Factors

In air quality management, emission estimates are necessary in order to design control strategies, evaluate sources and develop suitable mitigation techniques. An Emission Factor is "a representative value that attempts to relate the quantity of a pollutant released to the atmosphere with an activity associated with the release of that pollutant. These factors are usually expressed as the weight of pollutant divided by a unit weight, volume, distance, or duration of the activity emitting the pollutant" [19]. The currently available emission factors were developed using measurements from sources representing a certain area and/or conditions. Therefore, the available databases for emission factors may experience some limitations and inaccuracy when applied to the Middle East region.

II.3 Emission Inventories and Models

Emission inventories are an important ingredient of the growing effort to understand the impact of anthropogenic (i.e. human activities) and natural sources on air quality, particularly in the large urban areas. Emission inventories contain spatially and temporarily resolved emission data that help in determining the important emission sources in a geographical area and design or test the applicability of mitigation techniques. They also represent important input data to chemical transport models that simulate the atmospheric processes in order to provide a better understanding of the interactions between emissions, meteorology and atmospheric chemistry. Modern emission inventories cover larger domains, have fine temporal and spatial resolution and include a large variety of emission sources as well as many different chemical

compounds. Such anthropogenic emission inventories are available mostly for North America and Europe and some of them are listed below.

Pouliot et al. [12] presents the development of detailed emission inventories across North America and Europe in the framework of the Air Quality Model Evaluation International Initiative (AQMEII) project. The work included the generation of "model-ready" gridded emission datasets for 2006 across the two continental study domains. The study gives details about emission factors, spatial allocation, temporal variability and speciation of PM and VOCs. Moreover, the spatial and temporal distribution is compared for the following pollutants: NO_x, VOCs, SO_2, $PM_{2.5}$, CO, and NH_3. Emission estimates in both study domains are challenged by several important but poorly characterized emission source sectors, notably road dust, agricultural operations, biomass burning, and road transport. This work highlights also the similarities and differences in how emission inventories and datasets were developed and processed across North America and Europe.

Furthermore, Winiwarte [31] presents a review of emission inventories of particulate matter in Europe. A number of emission inventories have been developed for Europe and some of them are the Co-ordinated European Programme on Particulate Matter Emission Inventories, Projections and Guidance (CEPMEIP) inventory, the Greenhouse Gas and Air Pollution Interactions and Synergies (GAINS) dataset which is an independent Europe-wide top-down assessment and the European Monitoring and Evaluation Programme (EMEP) dataset. These emission inventories either focus on

specific sources such as road transport, domestic heating, industry, agriculture and natural sources or they include all sources for specific European regions.

Finally, a detailed European gridded emission inventory has been developed by the Netherlands Organization (TNO) [32] for the Monitoring Atmospheric Composition and Climate - Interim Implementation (MACC-II) project. MACC-II provides data records on atmospheric composition for recent years, data for monitoring present conditions and forecasts of the distribution of key constituents for a few days ahead. The TNO emission inventory is a European-wide, high resolution emission inventory for NO_x, CO, CH_4, NH_3, NMVOCs, SO_2, PM_{10}, $PM_{2.5}$ for the years 2003-2009. Emissions have been split in point sources and area sources and are available for all anthropogenic source categories.

A recent study by Waked [13] presents the development of a first temporally and spatially-resolved emission inventory for Lebanon. This inventory covers anthropogenic emission sources including (transport, energy production, agriculture… etc.) as well as biogenic emission sources from forests and grasslands. The inventory was based on emissions obtained for CO CO, NOx, SO_2, NMVOC, NH_3, PM_{10}, and $PM_{2.5}$ from 2010 year inventory. Industrial plants were found to be the major source of PM_{10} and $PM_{2.5}$ contributing to 59% of the PM_{10} and 57% of $PM_{2.5}$ emissions, followed by residential sector that contributes to 15% of PM_{10} and 20% of PM2.5 emissions. Another study by Waked and Afif [33] focused on the development of emission inventory for emissions from road transport in Lebanon. This latter was developed for a base year of 2010 using a bottom-up approach according to the guidelines of EEA/EMEP guidelines [34].

According to this study, road tire and surface wear are responsible for 55% of PM_{10} emissions. Although these traffic exhaust emissions continue to contribute to primary PM emissions in urban areas, non-exhaust emissions remains poorly characterized for the MEA.

PM emissions from natural sources play a significant role in the determination of air quality. Natural aerosols act cumulatively with particles of anthropogenic origin increasing the aerosol loading in urban centers especially those located close to large dust reservoirs such as deserts. Natural PM emissions in arid climate zones play an even more significant role in urban background pollution and should be taken into account in the study of the atmospheric pollution.

Regarding windblown dust, Zender [35] developed the mineral Dust Entrainment And Deposition (DEAD) model in order to study dust processes at both local and global scales. On the basis of the model results, the 1990s global annual windblown dust emissions have been estimated to be about 1490 Tg/year, lower than relevant estimations of previous studies. Laurent et al. [36] simulated Saharan dust emissions, transport and deposition using a regional model namely COSMO-MUSCAT (Consortium for Small-Scale Modeling-Multiscale Chemistry Aerosol Transport) within the Saharan Mineral Dust Experiment (SAMUM-1), which took place in May–June 2006. The Saharan dust emissions were estimated to be 78 Tg during the studied period.

Another significant work has been done by Nickovic [37], who developed the Dust Regional Atmospheric Model (DREAM). An updated version of DREAM called BSC-DREAM8b v2.0 has been developed and described in the studies of Perez et. al.

[38, 39], Basart et al. [40].The model predicts the atmospheric life cycle of the eroded desert dust.

In a recent study, Schaap et al. [41], presented the LOTOS-EUROS model which is an operational air quality and chemical transport model developed by TNO Built Environment and Geosciences and the National Institute for Public Health and the Environment (RIVM). The model includes a dust emission scheme and it simulates windblown dust emissions over Europe. Concerning sea salt emissions, a previous work of Gong and Barrie [42] described the simulation of the processes of sea salt aerosol production, transport and removal using the Canadian general climate model GCMII. This model was implemented in the North Atlantic between Iceland and Ireland. Another important study of the simulation of sea salt is that of Sofiev et al. [43]. The work presents a parameterization for sea salt emissions as well as its application in the SILAM dispersion modeling system for regional and global sea salt simulations. They found that the annual global production of sea salt aerosols is between 6700 and 7400 Tg/year.

CHAPTER III

METHODOLOGY

III.1 General Methodology

The fugitive PM releases from construction sector were examined in this study to provide the missing information in understanding the behavior of fugitive PM sources and their impact on public health in MEA. The main scope of the present study is to develop fugitive particulate matter emission factors for construction sites in MEA and to evaluate the accuracy of the existing emission factors to apply for Middle Eastern hot and arid conditions. An experimental campaign along with dispersion modeling using the Fugitive Dust Model (FDM) were implemented in a construction site to examine the relation between the meteorological variables, concentrations and emission rates to understand the behavior of the fugitive dust emissions for MEA. The experimental campaign was conducted on April-May, 2014 to get the PM contribution from a construction site (source) and a background location. The time period of this work was chosen while the construction site was at rest, where the only particles source was wind erosion of the loose soil. Particles concentrations were measured directly using an on-site monitoring tool. The FDM dispersion model was applied to estimate the source-receptor relation, using an initial value of 1 $g/m^2.s$ for the source emission rate. This value was chosen assuming that the emission rate is independent from the wind velocity for the initial run.

A data analysis was done, using the modeling results, to identify the effect of each meteorological variable (i.e. wind direction, wind speed, stability, .etc.) and its relation to emissions concentrations and rates. The data was classified by wind sector to identify the contributing sources. Considering the wind-speed dependence of the source emission rate, a power law function was obtained for the calculation of the emission rates. This function was used to re-run the FDM model and the results were evaluated compared to the on-site measured concentrations and to the emission factors reported in USEPA's AP-42 "Compilation of Air Pollutant Emission Factors" (the related emission rates in the latter emission inventory have been developed mainly for open coal-mines).

III.2 Monitoring Field Campaign

In this study, PM concentrations and meteorological data were measured on site using Environ Check 365#, an air quality monitoring station produced by Grimm Aerosol Technik GmbH & Co. KG, Germany (Figure 2). The air containing particles enters the station through a sampling-head and passes through a sampling pipe to enter a spectrometer. The sample air is directed into a measuring cell and detected by light scattering. The scattering light pulse for every single particle is being counted and the intensity of its scattering light signal classified to a certain particle size. The station measures particles over a size range of **0.25** up to **32 µm** in **31** size channels, and uses laser diode of 655 wavelengths as a light source [44].

Two monitoring stations were used for this study. One station was installed at a construction site located at Qatar Foundation Education City within the city of Doha, Qatar. The site was at rest during the campaign, where the only particles source was

Figure 2 Environ Check 365# air quality monitoring station (by Grimm Aerosol Technik GmbH & Co. KG, Germany)

wind erosion of the loose soil. It was chosen as it represents an open bare land, highly susceptible to wind activity and close to an educational campus & residential areas (Figure 3). The second station was placed on a roof top of a building located 1.5 km away (north east) from the first station, to measure background PM concentrations (Figure 4). PM emissions were monitored for a period of two months (April-May, 2014). A map showing the location of both stations is shown in (Figure 5).

The stations provide the count rate for each particle size as the number of particles per unit volume of the sample air (particles/liter). Meteorological data such as wind speed, wind direction, temperature and humidity were also measured through a climate sensor attached on the top of the station. All data were transmitted automatically from the stations to a computer network, and accessed through an online viewer. The data is also stored and can be extracted from an internal data logger inside the station.

Figure 3 Monitoring station installed at a construction site at rest

Figure 4 Monitoring station installed on a building rooftop at a background location

Figure 5 Map showing the locations and distance between the AQ stations

III.3 Atmospheric Dispersion Model

The Fugitive Dust Model (FDM) was used in this study. FDM is an air quality model designed specifically to compute emission concentrations and deposition impacts of fugitive dust sources [11]. The model is based on the Gaussian plume formulation but specifically adapted to incorporate an improved gradient-transfer deposition algorithm. Emissions of each source are split into a number of particle size classes, where a gravitational settling velocity and a deposition velocity are computed by the model for each class. The pollutant transport is ruled by the general atmospheric advection-diffusion equation. After a number of simplifying assumptions, the pollutant concentration is computed using the following equation:

$$\chi = \frac{Q}{2\pi\sigma_y\sigma_z u} e^{-\frac{y^2}{2\sigma_y^2}} e^{\left[\frac{-v_g(z-h)}{2K} - \frac{v_g^2\sigma_z^2}{8K^2}\right]} \left[e^{\frac{-(z-h)^2}{2\sigma_z^2}} + e^{\frac{-(z+h)^2}{2\sigma_z^2}} - \sqrt{2\pi}\frac{v_1\sigma_z}{K} e^{\left[\frac{v_1(z+h)}{K} + \frac{v_1^2\sigma_z^2}{2K^2}\right]} erfc\left[\frac{v_1\sigma_z}{\sqrt{2}K} + \frac{z+h}{\sqrt{2}\sigma_z}\right] \right] \quad \textbf{(1)}$$

where, χ is the pollutant concentration (g/m^3); $\mathbf{K_x}$, $\mathbf{K_y}$, $\mathbf{K_z}$ are the eddy diffusivity in the x, y and z directions (m^2/s); t is time (s); **u** is the wind speed (m/s); $\mathbf{v_g}$ is the gravitational settling velocity (m/s) where positive is in the downward direction. The **x**, **y**, **z** are the coordinates in three dimension space where **x** is parallel with the wind direction, **y** is perpendicular to x and parallel with the surface and **z** is perpendicular to both x and the surface (m) [11].

Concentrations and deposition rates are computed at all selected receptors. The main input data required to run the model, as shown in (Figure 6), include: meteorological data, sources information, receptors information and particles characteristics. The meteorological data is entered to the FDM model using any of the following three formats: (i) sequentially processed meteorological data set produced by the RAMMET pre-processor, (ii) card images of hourly meteorological data or (iii) a statistically-produced Stability ARay (STAR) [11]. The treatment of each of the input data within this work is explained in the remainder of this section.

III.3.1 Treatment of Meteorological Data

Short-term meteorological measurements (per minute) of wind speed, wind direction, humidity, pressure and temperature were provided by the on-site AQ monitoring station. These meteorological data were provided to the model using the card

images format. Two sets of FDM model calculations were done; once with 15-minute averaged values and one with 1-h averaged values of meteorological data.

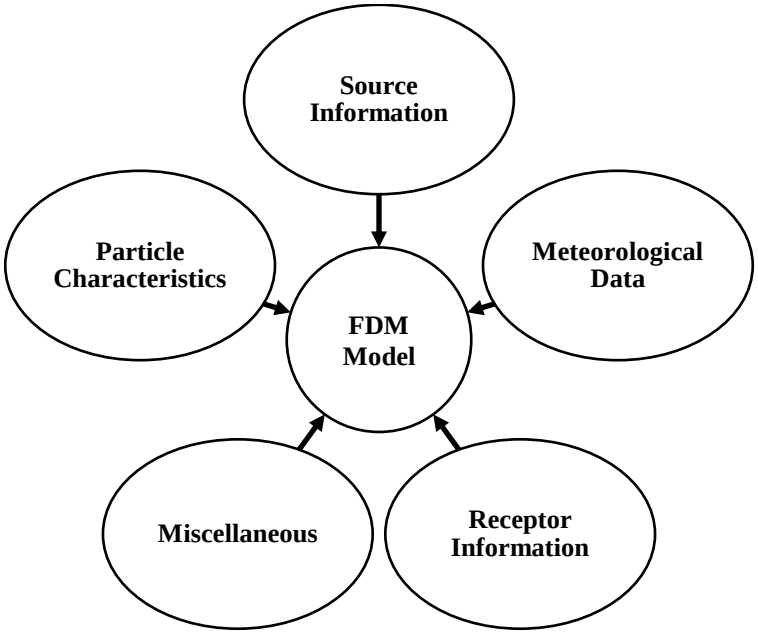

Figure 6 FDM input data

Before entering the meteorological data to the model, treatment of calms had to be done. Calms are defined as the periods with little or no air movement [45], or as defined in some references, the periods when the wind speed is less than 1 m/s. The steady state Gaussian plume models, such as FDM, do not apply in the periods of calms [9]. These models assume that the concentration is inversely proportional to wind speed, therefore the output concentrations become unrealistically large when the input wind speed to the model is less than 1 m/s. The procedure to treat these conditions concludes that site specific wind speed of less than 1 m/s but higher than the threshold of the

monitoring instrument should be entered to the model as 1 m/s [9]. For the periods of wind speeds less than the threshold of the instrument, meteorological data must be disregarded. In this study, the threshold wind speed of the monitoring station was 0.3 m/s.

Following the treatment of calms, 15-mintue averages and 1-h averages of meteorological data, except for wind direction, were directly calculated. Wind direction is a circular function of values between 1 and 360 degrees. Different treatment is needed to compute a valid mean value of the wind direction due to the discontinuity of wind direction at the beginning and end of the scale (i.e. at 0^o and 360^o) [45, 46]. The method developed by Mitsuta [46] was used in this work to estimate wind directions and compute the scalar mean wind direction. The standard deviation of the wind direction over the average periods was also calculated to be used for estimating the stability.

Atmospheric stability is a measure of the turbulent mixing capacity, and is represented by 6 classes labeled alphabetically from A to F, in which A is the least stable and F is the most stable [11]. Atmospheric Stability can be estimated using different methods. In this work, the turbulence-based ($\boldsymbol{\sigma_A}$) method that uses the standard deviation of wind direction and the scalar mean wind speed was used to estimate the stability [45]. This method starts with estimating an initial stability following the criteria shown in (Table 2), which is based on the standard deviation of the wind direction. The initial stability is then adjusted using the wind speed and the time of the day, as shown in (Table 3), to obtain the final stability for each unit of meteorological data. We must note here that the criteria in tables 3 and 4 is based on data collected at a measurement height

(Z=10 m) and a roughness length (z_o =15 cm). For a roughness length other than 15 cm, an adjustment of table 3 by multiplying the category boundaries with $(z_o/15)^{0.2}$ is needed. However, this adjustment is likely to be useful for cases when z_o is greater than 15 cm but is yet problematic whether it's as useful for when z_o is less than 15 cm. In this study, the roughness length is 0.06 cm, hence we choose not to implement this adjustment. Similarly, if the measurement height is other than 10 m, the category boundaries of table 3 need to be multiplied by $(Z/10)^{P\Phi}$, where the exponent P_Φ is a function of the stability categories with specified values. The measurement height in this work is estimated as 6 m; however the preceding adjustment was not made as it's likely to be useful for cases where Z is greater than 10 m.

Table 2 Lateral turbulence criteria for initial estimate of Pasquill-Gifford (P-G) stability category [45]

Initial estimate of P-G stability category	Standard deviation of wind azimuth angle σ_A
A	$22.5 \leq \sigma_A$
B	$17.5 \leq \sigma_A < 22.5$
C	$12.5 \leq \sigma_A < 17.5$
D	$7.5 \leq \sigma_A < 12.5$
E	$3.8 \leq \sigma_A < 7.5$
F	$\sigma_A < 3.8$

The mixing height was defined by Holzworth [47] as "height above the surface through which relatively vigorous vertical mixing occurs". Mixing height has significant

Table 3 Wind speed adjustments for determining final estimate of P-G stability category from σ_A[45]

Initial estimate of P-G Category		10 meter wind speed (m/s)	Final estimate of P-G Category
Daytime	**A**	**u < 3**	**A**
	A	**3 ≤ u < 4**	**B**
	A	**4 ≤ u < 6**	**C**
	A	**6 ≤ u**	**D**
	B	**u < 4**	**B**
	B	**4 ≤ u < 6**	**C**
	B	**6 ≤ u**	**D**
	C	**u < 6**	**C**
	C	**6 ≤ u**	**D**
	D, E, or F	**ANY**	**D**
Nighttime	**A**	**u < 2.9**	**F**
	A	**2.9 ≤ u < 3.6**	**E**
	A	**3.6 ≤ u**	**D**
	B	**u < 2.4**	**F**
	B	**2.4 ≤ u < 3.0**	**E**
	B	**3.0 ≤ u**	**D**
	C	**u < 2.4**	**E**
	C	**2.4 ≤ u**	**D**
	D	**ANY**	**D**
	E	**u < 5**	**E**
	E	**5 ≤ u**	**D**
	E		
	F	**u < 3**	**F**
	F	**3 ≤ u < 5**	**E**
	F	**5 ≤ u**	**D**

effect at distances far away from the source or in case of elevated receptors. In the case of fugitive dust, emissions are often released at or close to ground level, and consequently, mixing height has minimal effect on the predicted concentrations by FDM model [11]. Therefore, as shown in (Table 4), general values of mixing heights were assigned for each unit of meteorological data based on the stability class obtained.

Table 4 Mixing height based on stability class [11]

Stability Class	Mixing Height
A	**1,600**
B	**1,200**
C	**800**
D	**400**
E	**10,000**
F	**10,000**

III.3.2 Source Information

Emission sources can be categorized as point, line or area sources. FDM model can process up to 121 sources. Area sources need not be square but rather can be rectangular up to a ratio of (width to length) 1 to 5 [11]. In this work, the total area of the construction site has been divided into (23) smaller area sources as shown in (Figure 7). This way they are more representative of the total site area. The input information of each area source is shown in (Table 5).

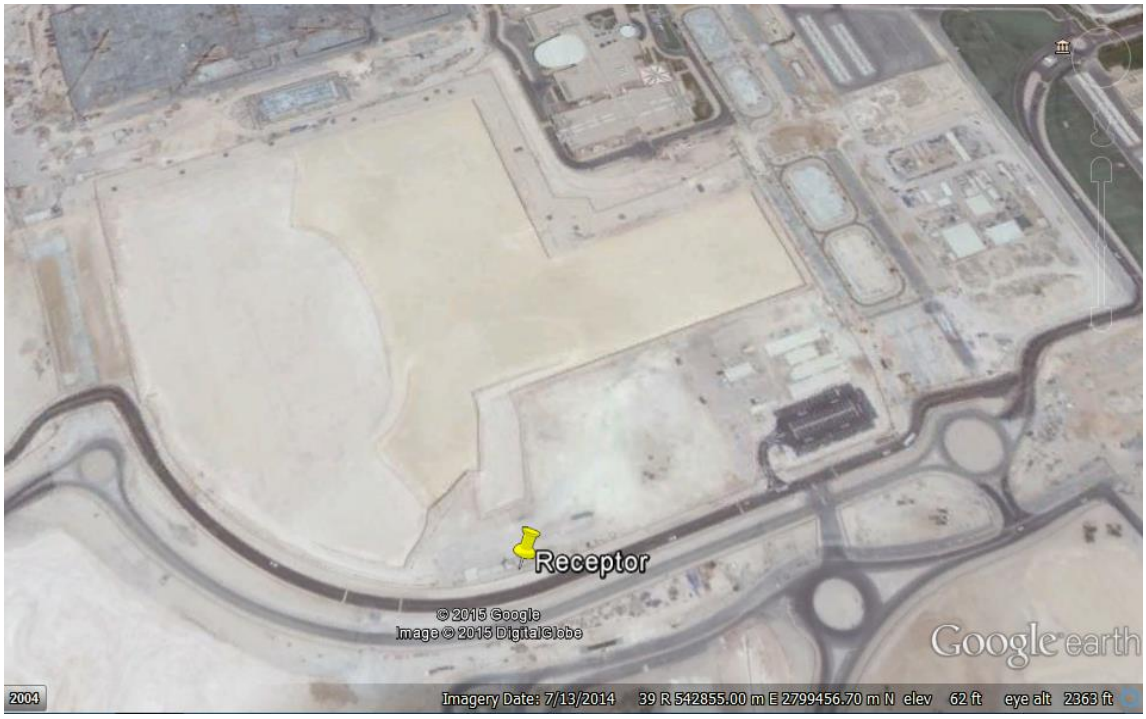

(a)

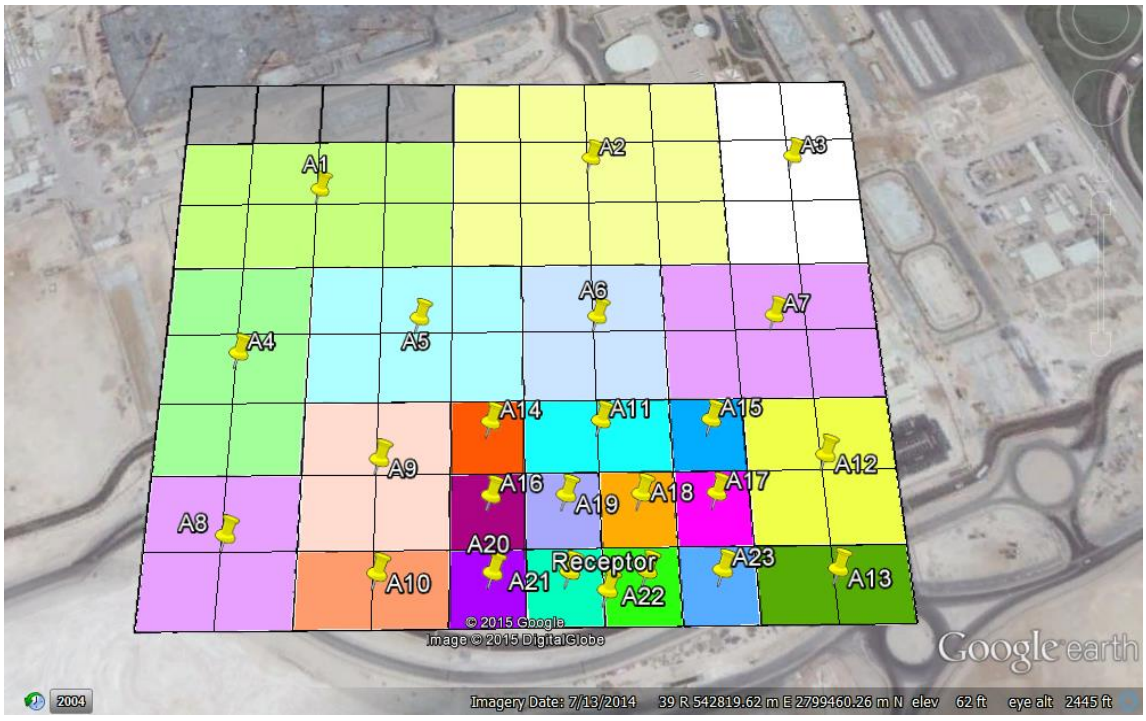

(b)

Figure 7 Site area (a) and the identified area sources (b) for the FDM

Table 5 Input data of each area source[1]

Area Source No.	X_1 (m)	Y_1 (m)	X_2 (m)	Y_2 (m)	Height (m)	Rotation Angle
1	542674.68	2799563.06	200.00	100.00	0.00	0.00
2	542874.53	2799588.36	200.00	150.00	0.00	0.00
3	543024.48	2799588.61	100.00	150.00	0.00	0.00
4	542624.86	2799438.01	100.00	150.00	0.00	0.00
5	542749.83	2799463.17	150.00	100.00	0.00	0.00
6	542874.77	2799463.42	100.00	100.00	0.00	0.00
7	542999.74	2799463.58	150.00	100.00	0.00	0.00
8	542625.11	2799313.07	100.00	100.00	0.00	0.00
9	542724.99	2799363.21	100.00	100.00	0.00	0.00
10	542725.07	2799288.23	100.00	50.00	0.00	0.00
11	542874.85	2799388.44	100.00	50.00	0.00	0.00
12	543024.88	2799363.70	100.00	100.00	0.00	0.00
13	543024.96	2799288.72	100.00	50.00	0.00	0.00
14	542799.89	2799388.27	50.00	50.00	0.00	0.00
15	542949.84	2799388.52	50.00	50.00	0.00	0.00
16	542799.97	2799338.29	50.00	50.00	0.00	0.00
17	542949.92	2799338.54	50.00	50.00	0.00	0.00
18	542899.94	2799338.45	50.00	50.00	0.00	0.00
19	542849.95	2799338.37	50.00	50.00	0.00	0.00
20	542800.05	2799288.31	50.00	50.00	0.00	0.00
21	542850.03	2799288.39	50.00	50.00	0.00	0.00
22	542900.02	2799288.47	50.00	50.00	0.00	0.00
23	542950.00	2799288.55	50.00	50.00	0.00	0.00

[1] **X1, Y1**: x and y coordinates of the center point of the area source
X2, Y2: x and y dimensions of the area source
Height: The release height for the emissions from the source
Rotation Angle: Number of degrees that the axis of the above x-dimension is rotated from the original x-axis of the map

III.3.3 Emission Rates

For the emission rates of fugitive dust which are often functions of the wind speed, the FDM model accounts for this proportionality by the following equation [11]:

$$E = Q_o u^w \quad \textbf{(2)}$$

where, "E**"** is the emission rate, "Q_0**"** is the proportionality constant, "u" is the wind speed and "w" is the wind speed dependence factor.

In this study, for every 15 min and then for every one hour, FDM model was run at first with an emission rate of 1 g/m^2.s for all sources. This value was chosen assuming that the emission rate is independent from the wind speed for the initial run (i.e. the wind speed dependence factor is set equal to zero). Also, the rate was assumed constant for all sources depending on the fact that the surface material is pretty much similar for all the 23 sources and under the same conditions.

III.3.4 Receptor Information

FDM can process up to 1200 receptor [11]. In this study, one receptor is considered; that is the air quality monitoring station located at the construction site. Receptor information is provided in (Table 6). The value of the z-coordinate represents the height of the receptor from the ground.

Table 6 Receptor information

Receptor Coordinates		
X (m)	**Y (m)**	**Z (m)**
542874.88	2799276.46	6

III.3.5 Particle Characteristics

Emissions from all sources are classified into a number of particle size classes. FDM can process up to 20 particle size classes [11]. In this study, the on-site monitoring stations measure particles over the size range of **0.25** up to **32 µm**. Hence, five particle size classes have been identified and are listed in (Table 7), with their corresponding diameter ranges. In this study, the model was run five times for each data set. Each run specifies a particle size class where the particles fraction for that class is set equal to one.

Table 7 Diameter range for each particle size class

Particle Size Class	Characteristics Diameter (µm)
1	0 - ≤ 2.5
2	>2.5 - ≤ 6
3	>6 - ≤10
4	>10 - ≤ 20
5	> 20 - ≤ 30

The FDM model requires the input of particle density, which varies depending on the type of the eroded material. Therefore, five soil samples have been collected from different parts of the construction site and tested in the lab to obtain the material density. The average density of the tested soil is 2.34 g/cm^3.

XRD and XRF tests have been also done for the same soil samples. The result of XRD analysis showed that the soil consisted mainly of Dolomite ($CaMg(CO_3)_2$), Calcite ($CaCO_3$) and Gypsum ($CaSO_4\ 2(H_2O)$).The average density of Dolomite is 2.84 g/cm^3,

2.71 g/cm^3 for Calcite and 2.31 g/cm^3 for Gypsum, which means that the value of density obtained from the lab tests is reasonable. Results of XRD and XRF tests are attached in Appendix B.

III.3.6 Miscellaneous

The other parameters entered as inputs to the FDM model such as surface roughness height, length of one unit of met data and number of hours of meteorological data processed is presented in (Table 8) below:

Table 8 Miscellaneous input parameters to FDM

Parameter	Entered Value
Number of hours of MET data processed	470 (15-minute averaged data) 114 (1-h averaged data)
Length (in minutes) of 1-unit of MET data (min) –	15 (15-minute averaged data) 60 (1-h averaged data)
Roughness length (cm)	0.06 (Desert- flat)

In (Table 8), the number of MET data processed represents the valid set of meteorological data, obtained during the two-month period experimental campaign, after the exclusion of calm periods, periods with invalid/error data and periods when the monitoring stations were at rest.

III.4 Evaluation of Emission Factors

The FDM model was first used to estimate the emission concentrations at the receptor point. An initial value of 1 g/m^2.s was assumed for the emission rate for the first run of the model. Initially, the model was set to compute the 15-minutes average

concentrations (μg/m^3) at the receptor point for each particle size class. Then, the model was set to compute the 1-h average concentrations (μg/m^3) at the same point and for each particle size class. The modeled concentration predicted by FDM is denoted in this context by (C_P).

The net value of the measured concentration, denoted by (C_M), is obtained for each particle size class by subtracting the concentration measured by the monitoring station at the background location (C_B) from the concentration measured at the receptor point (C_R):

$$C_M = C_R - C_B \quad \textbf{(3)}$$

Then, the measured and the predicted concentrations were used to estimate (correct) the emission rate for each time period, based on the linear relationship between the emission rate and the concentration. The corrected emission rate **(E`)** was calculated for each particle size class using the below proportionality:

$$E' = E\frac{C_M}{C_P} \quad \textbf{(4)}$$

The calculated emission rates were then classified based on their wind direction into twelve wind sectors of 30 degrees each. This classification aimed to filter the data in order to evaluate only the wind sectors covering the contributing sources, and then analyze the correlation between the emission rates and the meteorological parameters. The correlation between the emission rates, wind speed, wind direction, and stability were examined to identify the meteorological variables that affect the emission rates and provide the measure dependence for each variable.

The filtered emission rates were also plotted against the emission rates obtained using USEPA's AP-42 emission factors. This step aimed to evaluate the accuracy of the existing emission factors reported in AP-42 to apply for the MEA. It was important to identify the level of difference to be considered when developing new factors.

According to USEPA's AP-42, the following logarithmic law represents the wind speed profile in the surface boundary layer [19]:

$$u(z) = \frac{u*}{0.4} \ln \frac{z}{z_O} \quad \textbf{(5)}$$

where, "u" is the wind speed, "u*" is the friction velocity, z is the height above test surface, z_o is the roughness height and the 0.4 is the von Karman's constant.

Equation (5) was used to calculate the friction velocity. The erosion potential for a dry exposed surface is calculated using the below equation [19]:

$$P = 58(u^* - u_t^*)^2 + 25(u^* - u_t^*) \quad \textbf{(6)}$$

where, P_i is the erosion potential (g/m^2), and u_t is the threshold friction velocity.

The wind-generated particulate emissions from a surface consisting of both erodible and non-erodible material can be estimated using the below emission factor equation [19]:

$$EF = k \sum_{i=1}^{N} P_i \quad \textbf{(7)}$$

where, EF is the emission factor (g/m^2), k particle size multiplier, N is the number of disturbances per year.

Finally, the emission rates obtained from FDM were plotted against the wind speed, for each particle size class, to obtain the corrected emission rate functions. This is based on the wind-speed dependence represented by equation (2), and giving that the wind speed is the factor that contributes the most to particles entrainment. These functions were then used to re-run the FDM model in order to evaluate the results against the on-site measured concentrations. The results of this study are presented in the next chapter.

CHAPTER IV

RESULTS & DISCUSSION

In this chapter, the results of the study are presented. Initially, graphs were obtained to demonstrate the concentration change in relation with the wind speed; the factor that contributes the most to particles entrainment. Time series plots of the measured concentrations and wind speed at the receptor point over the whole study period are shown in (Figure 8).

As shown in (Figure 8), the concentration peaks correspond to the wind speed peaks, and the gaps in the plot show the periods where the monitoring station was off.

Next, time series plots were done as shown in (Figure 9) to compare the measured concentrations at the receptor and background location for three particle size classes. The deviations between the concentrations at the receptor and the background location show different behavior at some points. This is probably because the background station location was selected too far away from the receptor, which may be affected by factors that did not affect the construction site.

The meteorological measurements and concentrations at the receptor point and the background location were compared in order to examine the correlation between all variables. This comparison was done based on the 15-minute averaged data. A high correlation (between 0.7-0.9) was observed between the concentrations of different size classes in both locations. This means that all particle classes are strongly related and the

largest fraction is affected by the same sources. The correlation table is shown in Appendix C.

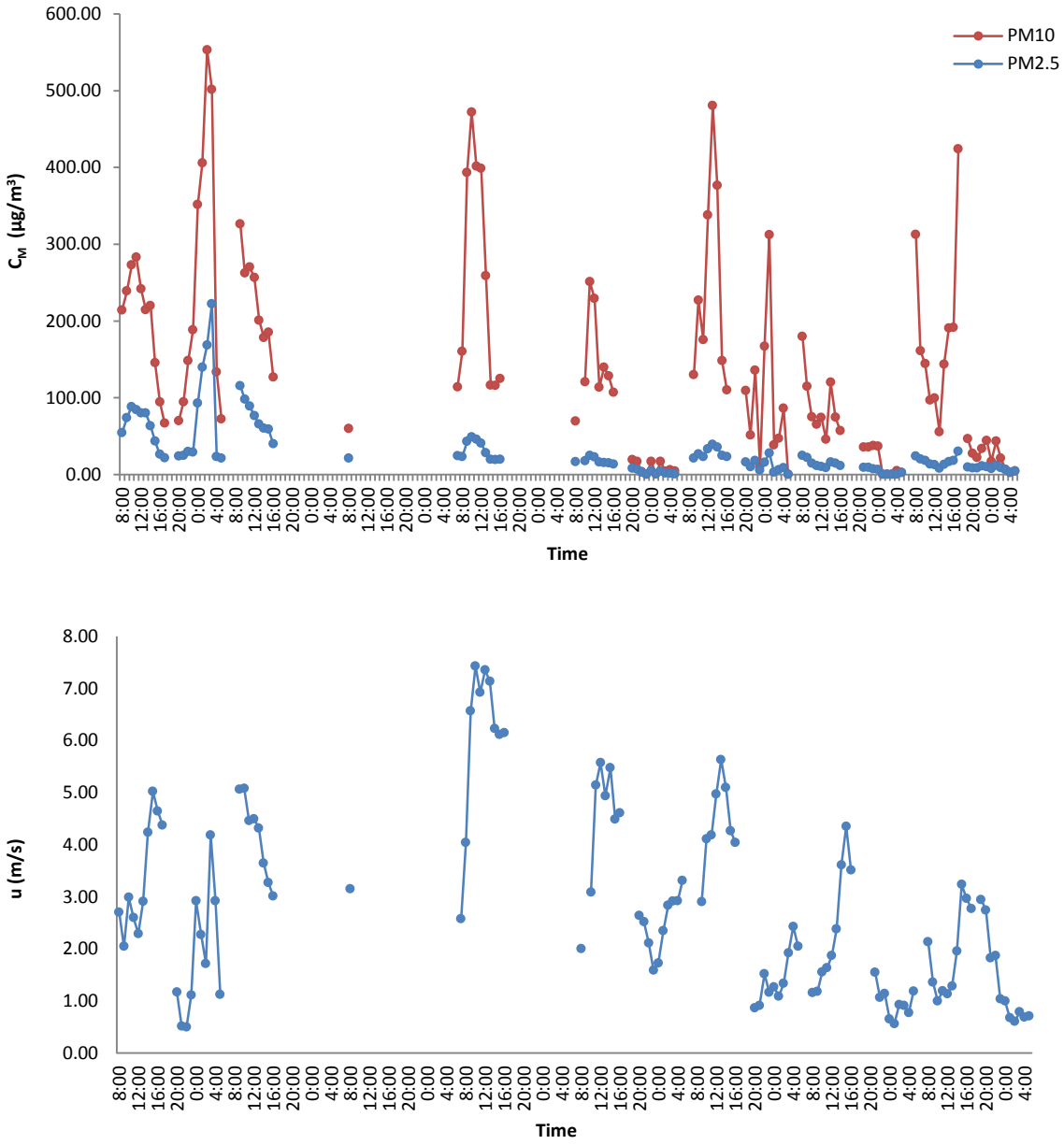

Figure 8 Time series of the measured PM concentrations and wind speed

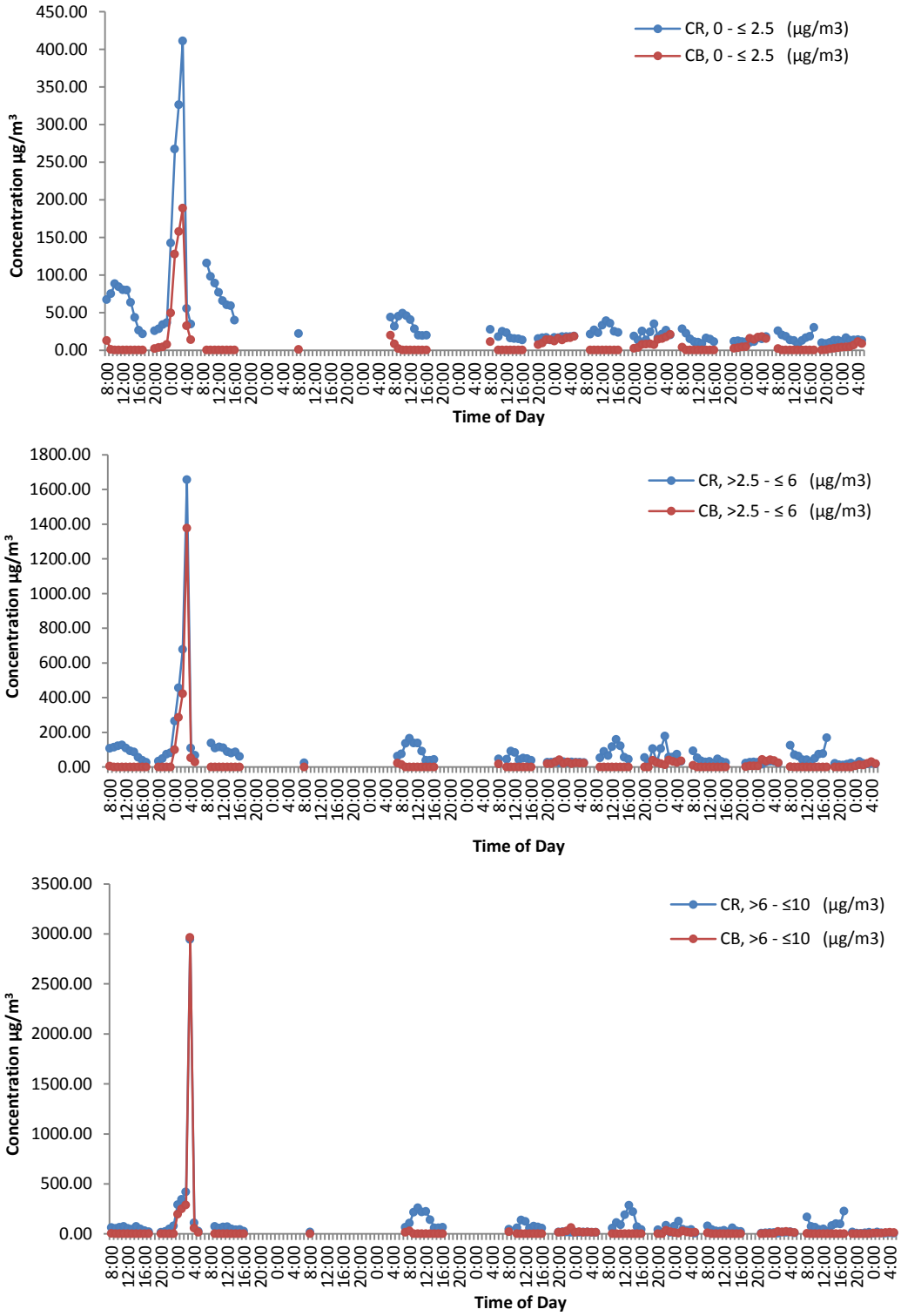

Figure 9 Comparison between the measured concentrations at the receptor and background

In parallel, there is a significant difference between the construction site and background measurements. Therefore, it was considered a safe assumption that the construction site produces the majority of the measured particles. Similarly, it was assumed that the background location is not affected by a single source. Finally, this means that, both locations are affected by sources that have very similar size profile; construction activities and natural dust are our estimation.

In addition, the emission rates were compared with the meteorological measurements from construction site and the background location. This comparison was done for both, 15-minutes and 1-h averaged data. The results based on the 15-minutes averages showed a relatively good correlation between the emission rates and wind speeds, especially for the smaller particles (<10 $\mu g/m^3$). This correlation was even higher when using the hourly averages. This is an expected result since the wind speed is the main factor that induces the particles. The correlation tables are shown in Appendix D.

Some results based on the hourly averages showed higher correlation between the emission rates for the small particles (0-6 $\mu g/m^{3)}$ and the background wind speed, and between the larger particles (6-30 $\mu g/m^3$) and the receptor wind speed. This means that probably the smaller particles are coming from the background and the larger particles are coming from the construction site. Also, for the 15 minute averages, the wind direction did not follow the expected pattern, and hence did not give clear information about its effect on the emission rates.

The emission rates obtained from FDM were plotted against the wind speed for three particle size classes (up to PM_{10}), as shown in (Figures 10, 11 and 12). These plots

were made to obtain the power functions for the emission rate. These functions provide the developed emission rates and wind dependence factors.

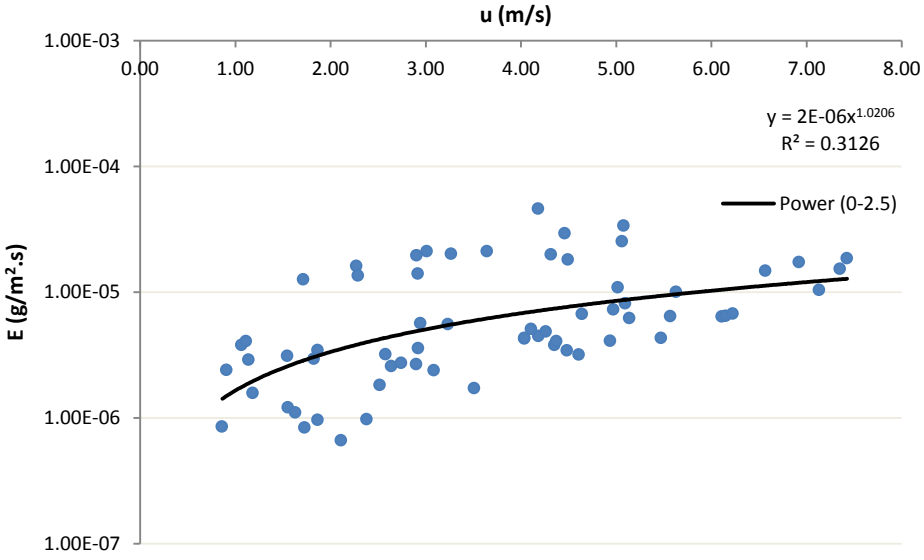

Figure 10 The emission rate-wind speed relation for the (0-2.5 µm) size class

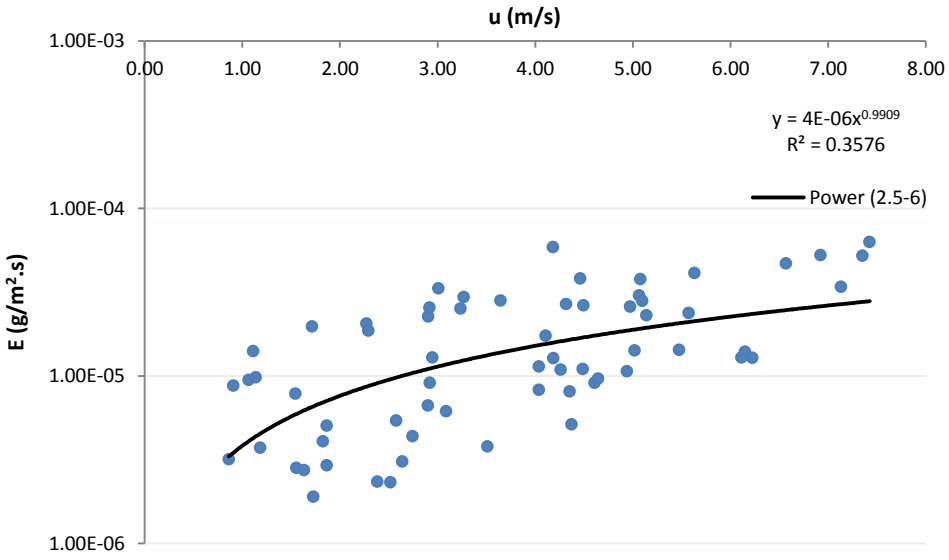

Figure 11 The emission rate-wind speed relation for the (2.5-6 µm) particle size class

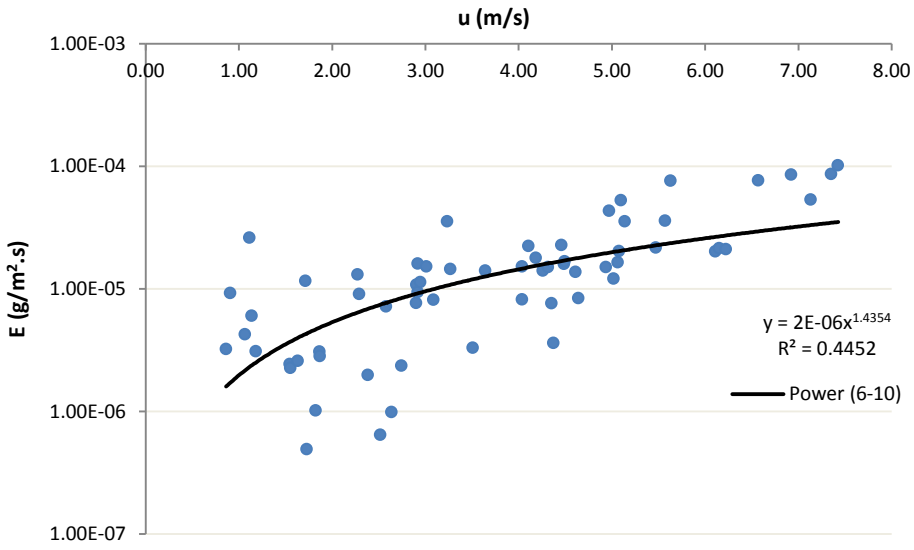

Figure 12 The emission rate-wind speed function for (6-10 µm) particle size class

Then, FDM model was re-executed with the new emission rates. Three separate runs were made for each particle size class (0-2.5 µm, 2.5-6 µm and 6-10 µm). The new model results were combined to obtain $PM_{2.5}$ and PM_{10} concentrations.

In order to evaluate our new emission rates, these were compared with the commonly used AP-42 emission factors. It is important to note that the AP-42 emission factors, for this type of sources have been developed for open coal-mines.

Both emission rates were plotted against the wind speed, as shown in (Figures 13 and 14). As shown in these figures, there is a good level of agreement between the model emission rates and the ones obtained from AP-42, which indicates that the emission factors reported in USEPA's AP-42 could apply, with a good level of accuracy, for the case of the bare land wind erosion in the MEA.

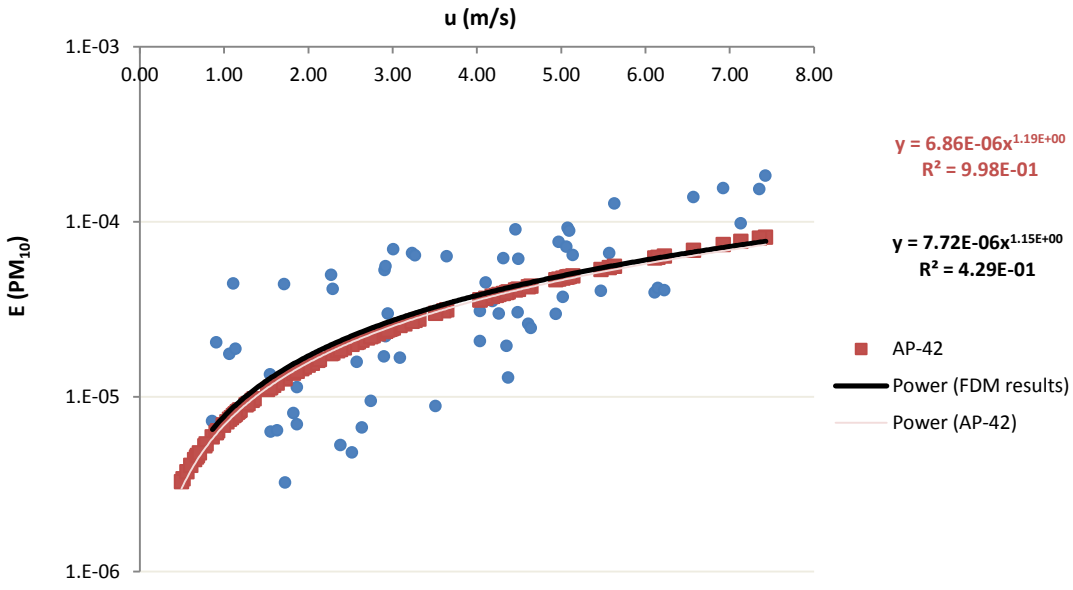

Figure 13 Comparison between this study's and AP-42 emission rates for $PM_{2.5}$

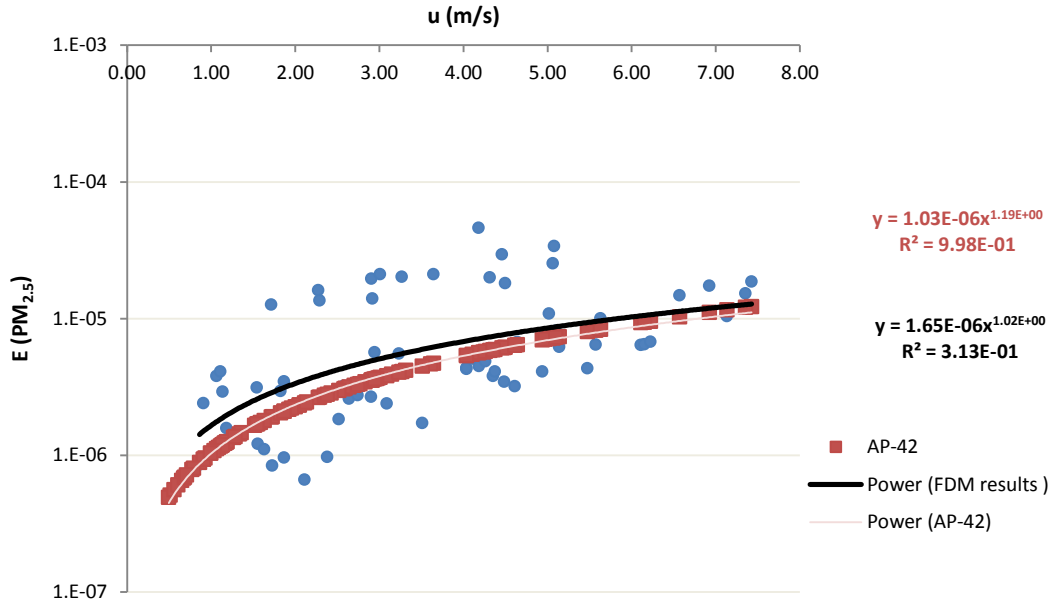

Figure 14 Comparison between this study's and AP-42 emission rates for PM_{10}

Following the FDM re-execution, times series of the resulted concentrations as well as the measured concentrations were plotted, as shown in (Figures15 and 16), to compare the new results of the model and the measured concentration.

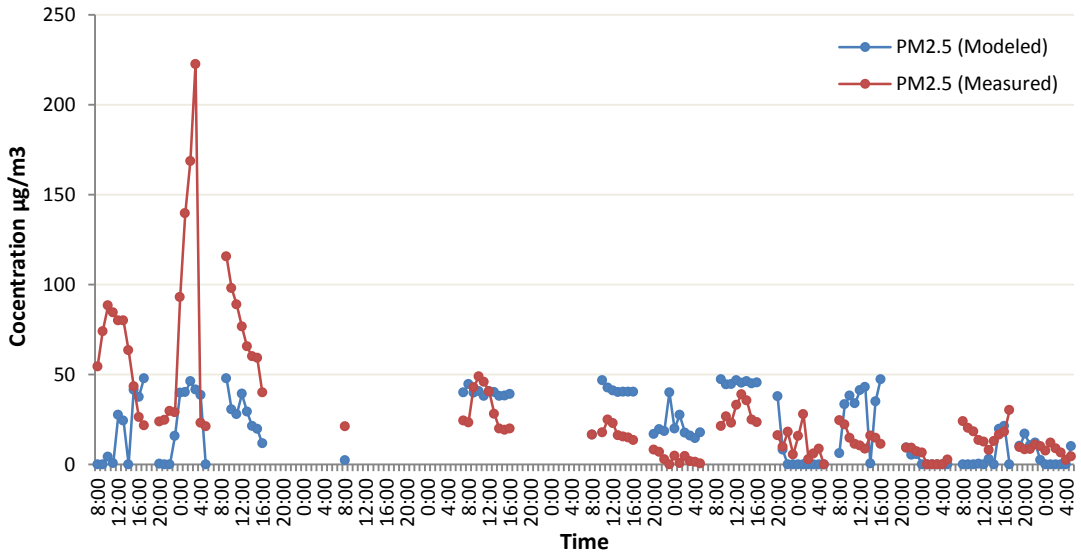

Figure 15 Time series of the modeled and measured concentrations for $PM_{2.5}$

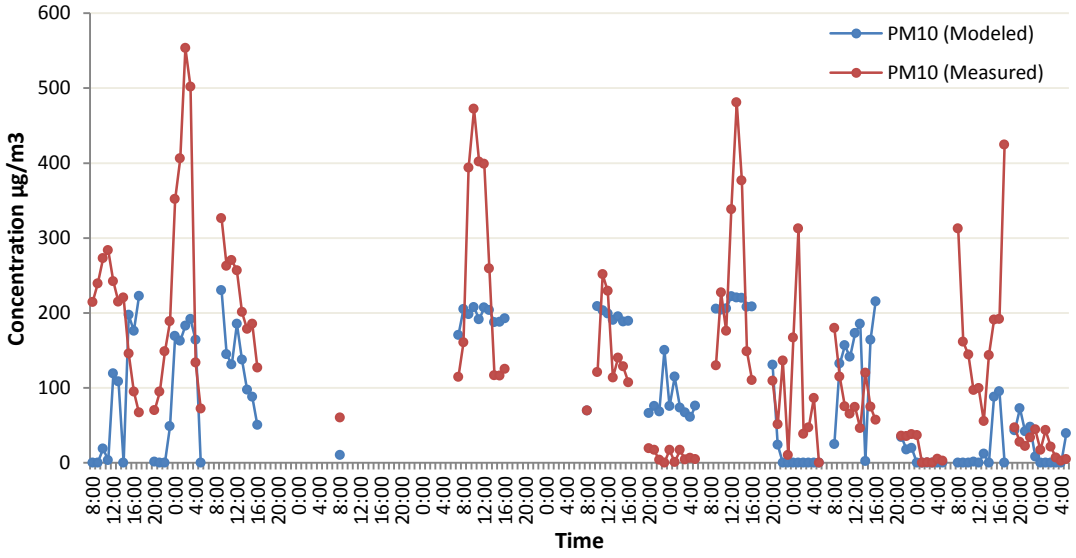

Figure 16 Time series of the modeled and measured concentrations for PM_{10}

It can be observed from the previous plots that the measured concentrations are higher than the concentrations computed by the model which do not exceed 200 $\mu g/m^3$. The reason for this is that the model accounts only for the input sources while the measured concentrations could include contributions from other sources around the study area.

Finally, the concentrations computed by the FDM model were plotted against the measured concentrations for comparison. The concentrations were also filtered by wind sector to plot the concentrations covering only the contributing sources. The results are shown in (Figures 17 and 18).

The blue points shown in the plots represent the relation between the modelled and measured concentrations using all the data. The red points, however, demonstrate only the concentrations within the wind sectors affected by the source. The blue points laying on the axis indicate the wind sectors that are not affected by the studied sources.

The graphs shown in (Figures 17 and 18) present the level of agreement between the measured concentrations and the concentrations obtained using the dispersion modeling. The results are acceptable and between the lines that show for a factor of two how close the modeled results are compared to the measurements. The statistical metric of factor-of-two (FAC2) is a common one for dispersion modeling.

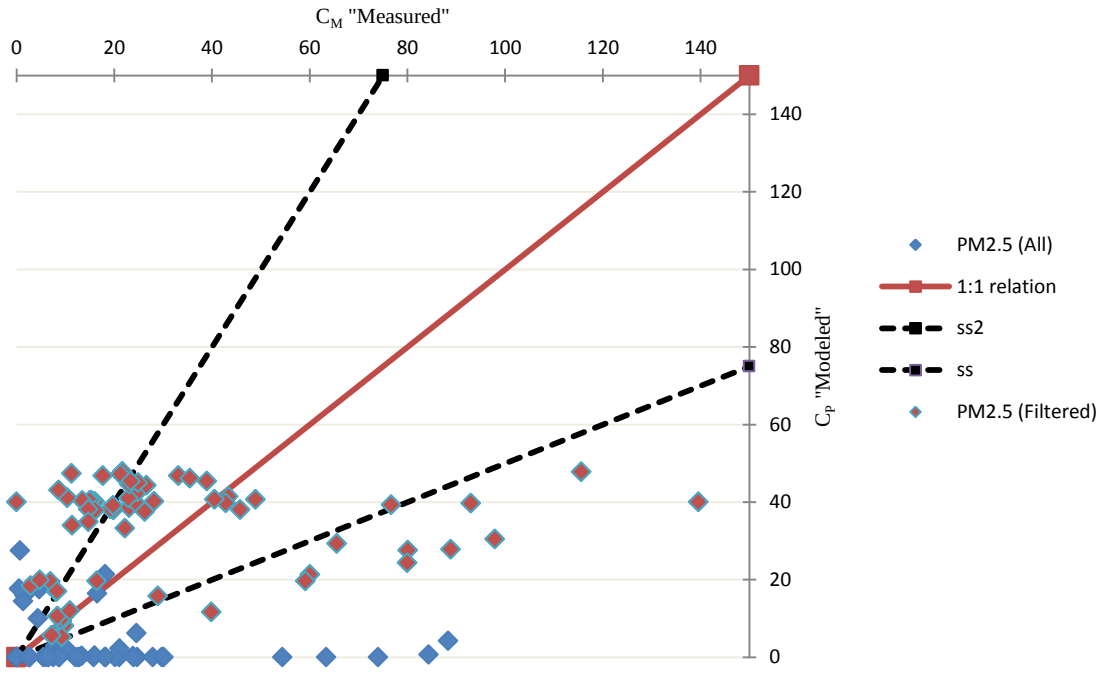

Figure 17 The modeled versus the measured concentrations for $PM_{2.5}$

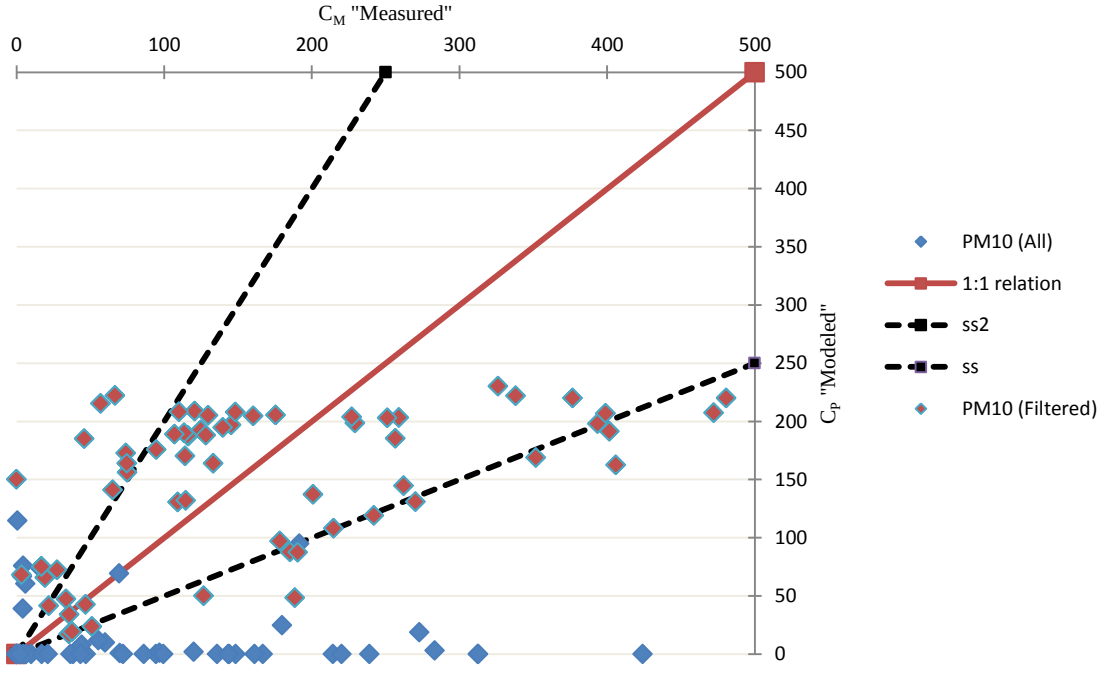

Figure 18 The modeled versus the measured concentrations for PM_{10}

CHAPTER V

CONCLUSIONS

V.1 Conclusions

The releases of airborne PM from major building activities such as building construction is largely unknown for the Middle East area. In the present study, fugitive PM releases from a construction site in Middle East area were examined.

PM concentrations from the experimental campaign along with the FDM model results were used to correlate meteorological variables, concentrations and emission rates to understand the behavior of the fugitive dust emissions. In this study the fugitive PM emission factors reported in USEPA AP-42 "Compilation of Air Pollutant Emission Factors" were determined and new emission rate relationships were developed to apply for Middle Eastern conditions.

Surprisingly, our study showed that a very good agreement between the AP-42 emission factors and our calculations can be obtained if the former are slightly modified. The emission factors developed in this study have been confirmed and can be applied for the impact assessment of similar sources in Middle East and other dry-arid locations. Also, the wind speed and stability are the main meteorological factors affecting the emission rates.

V.2 Future Work

A future work plan is going to be performed by a comprehensive study of fugitive PM emissions from different sources in the Middle East area, in order to

develop new emission inventories applicable for dry and arid regions dominated by fugitive PM. Sources to be studied include construction activities (building, recycling and demolition), natural sources (wind-blown dust, sea salt), and road traffic (breaks, street surface, tire abrasion and dust re-suspension). More field studies, lab work and emission modeling will be conducted to develop a comprehensive understanding of the fugitive PM behavior and its impacts on air quality and public health. Field studies for construction activities and traffic sources will collect source related information and atmospheric measurements of ambient size resolved PM. Chemical characterization of the collected PM samples during these field studies, together with the use of receptor models, will accomplish the source apportionment and contribution by individual PM sources. The ultimate goal will be to develop an online emission inventory that will provide essential background information for use in Air Quality Management systems (dispersion models) and will be one of the most useful tools for the development of abatement strategies and policies for the State of Qatar as well as the wider Middle East Area.

REFERENCES

1. Tsiouri, V., Kakosimos, K.E., and Kumar, P., *Concentrations, sources and exposure risks associated with particulate matter in the Middle East area-a review.* Air Quality, Atmosphere & Health, 2014: p. 1-14.

2. Shao, Y., *Physics and modelling of wind erosion*. Atmospheric and Oceanographic Sciences Library, ed. L.A. Mysank, Department of Atmospheric and Oceanographic Sciences, McGill University, Montreal, Canada and K. Hamilton, International Pacific Research Center, University of Hawaii, Honolulu, HI, U.S.A. Vol. 37. 2009: S.l. : Springer.

3. Bu-Olayan, A.H. and Thomas, B.V., *Dispersion model on PM 2.5 fugitive dust and trace metals levels in Kuwait governorates.* Environmental Monitoring and Assessment, 2012. **184**(3): p. 1731-1737.

4. Engelbrecht, J.P. and Jayanty, R.K.M., *Assessing sources of airborne mineral dust and other aerosols, in Iraq.* Aeolian Research, 2013. **9**: p. 153-160.

5. Rashki, A., et al., *Assessment of chemical and mineralogical characteristics of airborne dust in the Sistan region, Iran.* Chemosphere, 2013. **90**(2): p. 227-236.

6. Pope lll, C.A. and Dockery, D.W., *Health effects of fine particulate air pollution: lines that connect.* Journal of the Air & Waste Management Association, 2006. **56**(6): p. 709-742.

7. Chen, R., et al., *Association of particulate air pollution with daily mortality: the China air pollution and health effects study.* American Journal of Epidemiology, 2012. **175**(11): p. 1173-1181.

8. Neuman, C.M., Boulton, J.W., and Sanderson, S., *Wind tunnel simulation of environmental controls on fugitive dust emissions from mine tailings.* Atmospheric Environment, 2009. **43**(3): p. 520-529.

9. USEPA, *Revision to the guideline on air quality models: adoption of a preferred general purpose (flat and complex terrain) dispersion model and other revisions.* US Environmental Protection Agency, 2005. **70**(216): p. 68218-68261.

10. Abdul-Wahab, S.A., *Impact of fugitive dust emissions from cement plants on nearby communities.* Ecological Modelling, 2006. **195**(3–4): p. 338-348.

11. Winges, K.D., *User's guide for the Fugitive Dust Model (FDM) revised: user's instructions.* US Environmental Protection Agency, Report (EPA-910/9-88-202R); TRC Environmental Consultants, 1991.

12. Pouliot, G., et al., *Comparing emission inventories and model-ready emission datasets between Europe and North America for the AQMEII project.* Atmospheric Environment, 2012. **53**(0): p. 4-14.

13. Waked, A., Afif, C., and Seigneur, C., *An atmospheric emission inventory of anthropogenic and biogenic sources for Lebanon.* Atmospheric Environment, 2012. **50**(0): p. 88-96.

14. Kon, L.C., Durucan, S., and Korre, A., *The development and application of a wind erosion model for the assessment of fugitive dust emissions from mine tailings dumps.* International Journal of Mining, Reclamation and Environment, 2007. **21**(3): p. 198-218.

15. *Emission estimation technique manual for cement manufacturing* in *National Pollutant Inventory (NPI).* 1999, Australian Government, Department of the Environement.

16. Ono, D., et al., *Application of a combined measurement and modeling method to quantify windblown dust emissions from the exposed playa at Mono Lake, California.* Journal of the Air & Waste Management Association, 2011. **61**(10): p. 1036-1045.

17. Sanderson, R.S., Neuman, C.M., and Boulton, J.W., *Windblown fugitive dust emissions from smelter slag.* Aeolian Research, 2014. **13**(0): p. 19-29.

18. Kinsey, J.S., et al., *Characterization of the fugitive particulate emissions from construction mud/dirt carryout.* Journal of the Air & Waste Management Association, 2004. **54**(11): p. 1394-1404.

19. USEPA, *Emissions factors & AP 42, compilation of air pollutant emission factors* 1995, U.S. Environmental Protection Agency.

20. Park, Y.-K. and Park, S.H., *Development of a new wind-blown-dust emission module using comparative assessment of existing dust models.* Particulate Science and Technology, 2010. **28**(3): p. 267-286.

21. Vesovic, V., Auziere, A., Calviac, G., and Dauriat, A., *Modelling of the dispersion and deposition of coarse particulate matter under neutral atmospheric conditions.* Atmospheric Environment, 2001. **35**(1): p. S99-S105.

22. Heal, M.R., Kumar, P., and Harrison, R.M., *Particles, air quality, policy and health.* Chemical Society Reviews, 2012. **41**(19): p. 6606-6630.

23. Chen, L.C. and Lippmann, M., *Effects of metals within ambient air particulate matter (PM) on human health.* Inhalation Toxicology, 2009. **21**(1): p. 1-31.

24. Gibson, J.M., et al., *Deaths and medical visits attributable to environmental pollution in the United Arab Emirates.* PLoS ONE, 2013. **8**(3).

25. Pope, J. *Qatar's construction sector*. WWL-WHO'SWHOLEGAL, 2011.

26. Dorevitch, S., et al., *Demolition of high-rise public housing increases particulate matter air pollution in communities of high-risk asthmatics.* Journal of the Air & Waste Management Association, 2006. **56**(7): p. 1022-1032.

27. Kumar, P., Mulheron, M., and Som, C., *Release of ultrafine particles from three simulated building processes.* Journal of Nanoparticle Research, 2012. **14**(4): p. 1-14.

28. Holmes, N.S. and Morawska, L., *A review of dispersion modelling and its application to the dispersion of particles: An overview of different dispersion models available.* Atmospheric Environment, 2006. **40**(30): p. 5902-5928.

29. Kumar, P., et al., *Dynamics and dispersion modelling of nanoparticles from road traffic in the urban atmospheric environment-a review.* Journal of Aerosol Science, 2011. **42**(9): p. 580-603.

30. Babu, C.A., Samah, A.A., and Varikoden, H., *Rainfall climatology over Middle East region and its variability.* International Journal of Water Resources & Arid Environments, 2011. **1**(3): p. 180-192.

31. Winiwarter, W., Kuhlbusch, T.A.J., Viana, M., and Hitzenberger, R., *Quality considerations of European PM emission inventories.* Atmospheric Environment, 2009. **43**(25): p. 3819-3828.

32. Kuenen, J., et al., *MACC European emission inventory for the years 2003-2007*. 2011.

33. Waked, A. and Afif, C., *Emissions of air pollutants from road transport in Lebanon and other countries in the Middle East region.* Atmospheric Environment, 2012. **61**(0): p. 446-452.

34. EEA, *EMEP/EEA air pollutant emission inventory guidebook*. 2009, European Environment Agency (EEA).

35. Zender, C.S., Bian, H., and Newman, D., *Mineral Dust Entrainment and Deposition (DEAD) model: description and 1990s dust climatology.* Journal of Geophysical Research D: Atmospheres, 2003. **108**(14): p. AAC 8-1 - AAC 8-19

36. Laurent, B., et al., *A model study of Saharan dust emissions and distributions during the SAMUM-1 campaign.* Journal of Geophysical Research: Atmospheres, 2010. **115**(21).

37. Nickovic, S., Kallos, G., Papadopoulos, A., and Kakaliagou, O., *A model for prediction of desert dust cycle in the atmosphere.* Journal of Geophysical Research: Atmospheres, 2001. **106**(16): p. 18113-18129.

38. Perez, C., et al., *A long Saharan dust event over the western Mediterranean: Lidar, Sun photometer observations, and regional dust modeling.* Journal of Geophysical Research: Atmospheres, 2006. **111**(15).

39. Pérez, C., et al., *Interactive dust-radiation modeling: A step to improve weather forecasts.* Journal of Geophysical Research: Atmospheres, 2006. **111**(16).

40. Basart, S., et al., *Development and evaluation of the BSC-DREAM8b dust regional model over northern Africa, the Mediterranean and the Middle East.* Tellus Series B-Chemical and Physical Meteorology, 2012. **64**(0): p. 1-23.

41. Schaap, M., et al., *Regional modelling of particulate matter for the Netherlands*. 2009, Netherlands Environmental Assessment Agency, (PBL).

42. Gong, S.L., Barrie, L.A., and Blanchet, J.P., *Modeling sea-salt aerosols in the atmosphere. 1. Model development.* Journal of Geophysical Research: Atmospheres, 1997. **102**(3): p. 3805-3818.

43. Sofiev, M., et al., *A regional-to-global model of emission and transport of sea salt particles in the atmosphere.* Journal of Geophysical Research: Atmospheres, 2011. **116**(21).

44. Grimm, *Manual, Environ Check 365*. Grimm Aerosol Technik GmbH & Co. KG, Germany.

45. USEPA, *Meteorological monitoring guidance for regulatory modeling applications*. 2000: U.S. Environmental Protection Agency, Office of Air and Radiation, Office of Air Quality Planning and Standards, Research Triangle Park, NC.

46. Mori, Y., *Evaluation of several 'single-pass' estimators of the mean and the standard deviation of wind direction.* Journal of Climate and Applied Meteorology, 1986. **25**(10): p. 1387-1397.

47. Holzworth, G.C., *Mixing heights, wind speeds, and potential for urban air pollution throughout the contiguous United States*. 1972: U.S. Environmental Protection Agency, Office of Air Programs, Research Triangle Park, NC.

APPENDIX A

MEASUREMENTS OF AQ STATIONS

Measured meteorological data and PM concentrations that were collected during the experimental campaign (as discussed in Chapter III) and used in this study are included in a separate file.

APPENDIX B

XRD AND XRF RESULTS OF SOIL SAMPLES

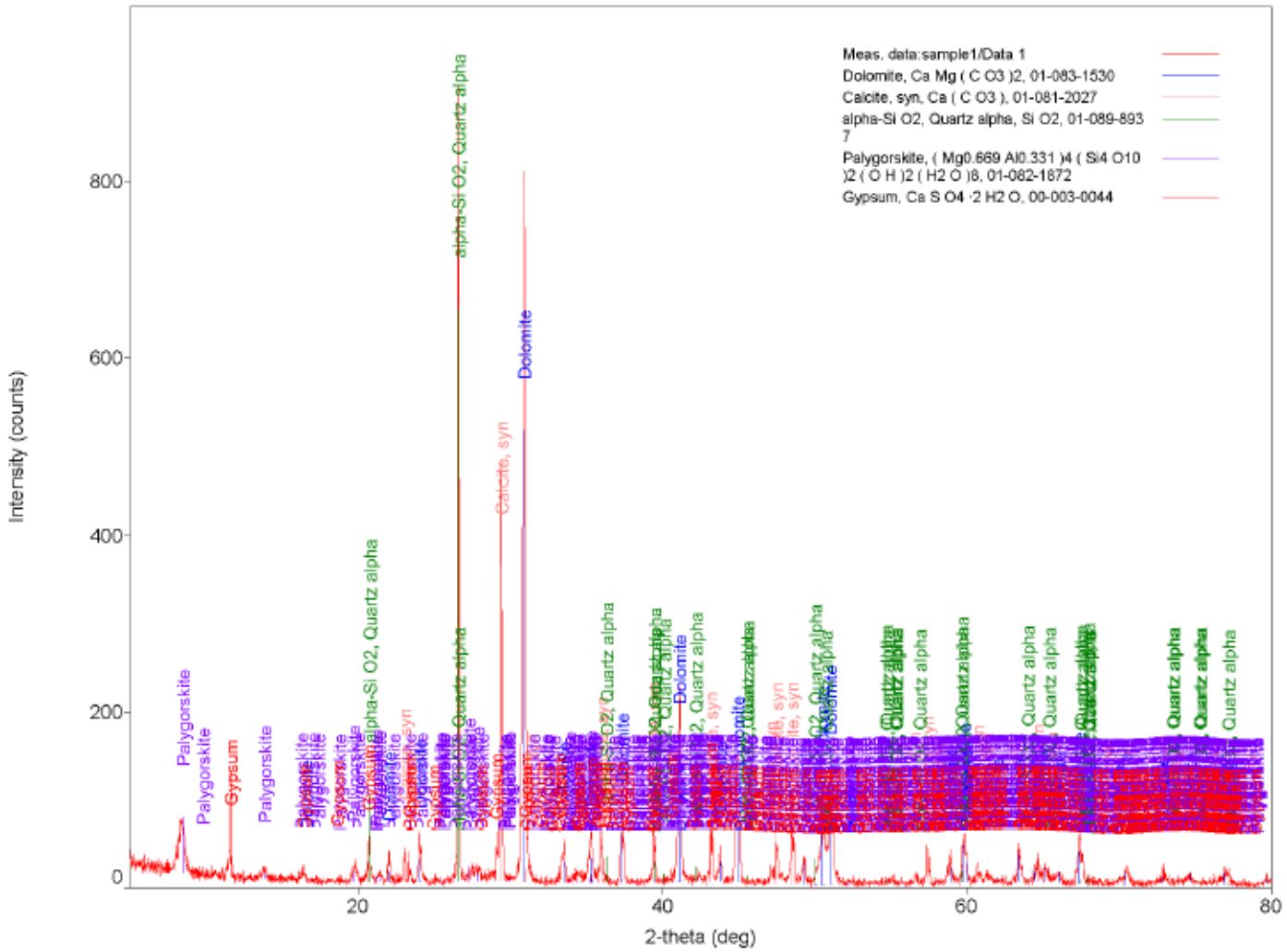

Figure B-1 XRD graph of sample (1)

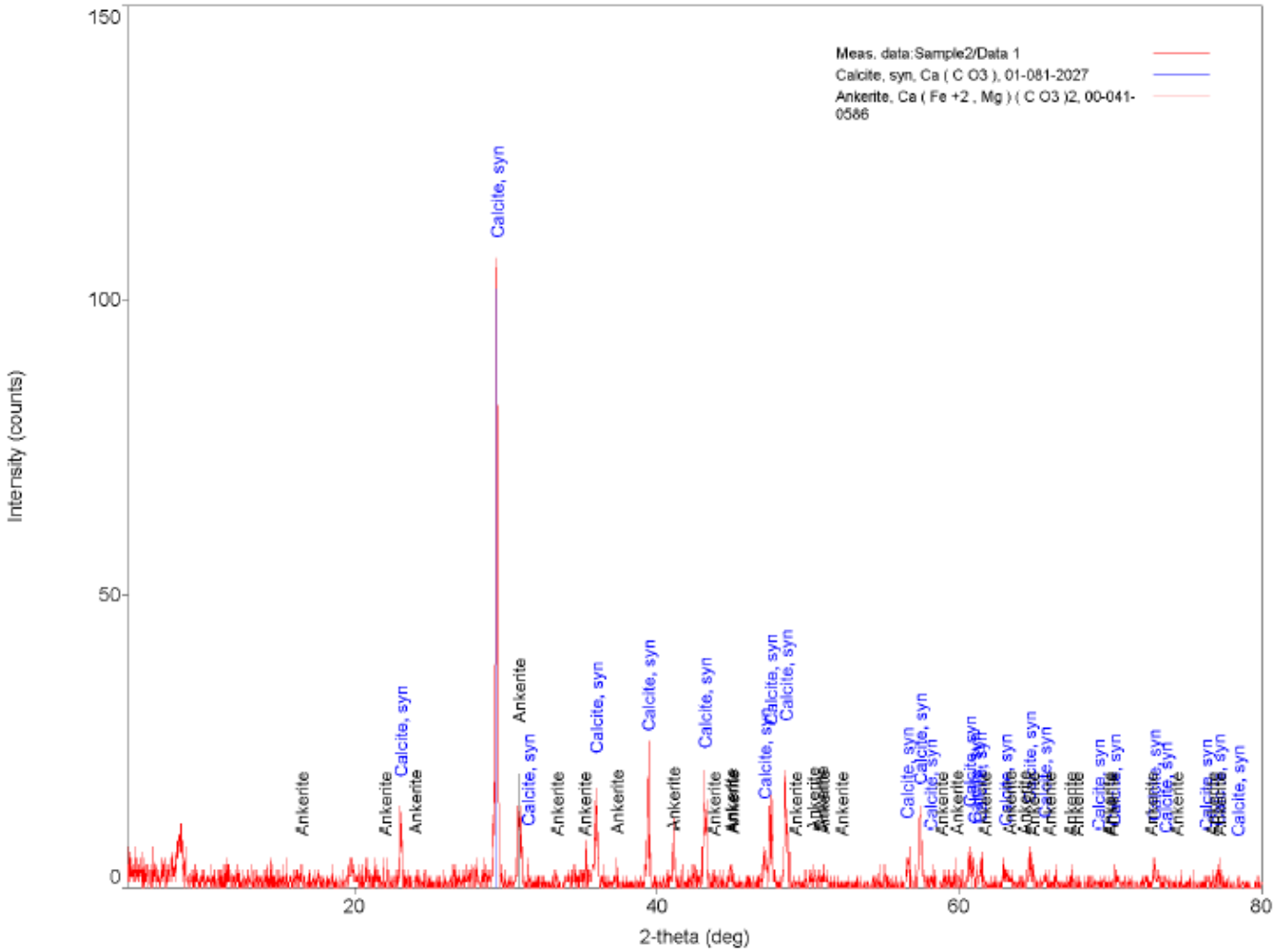

Figure B-2 XRD graph of sample (2)

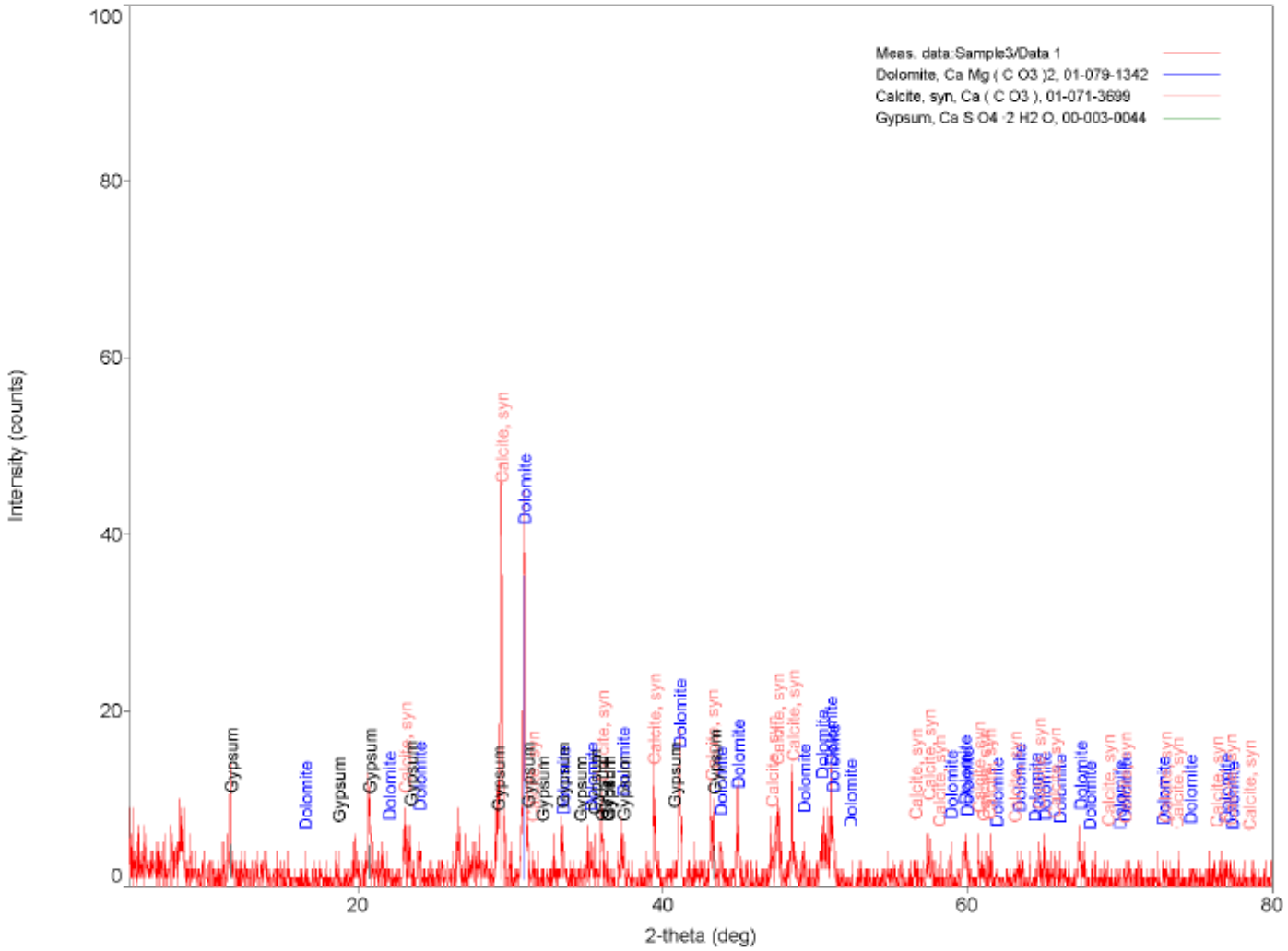

Figure B-3 XRD graph of sample (3)

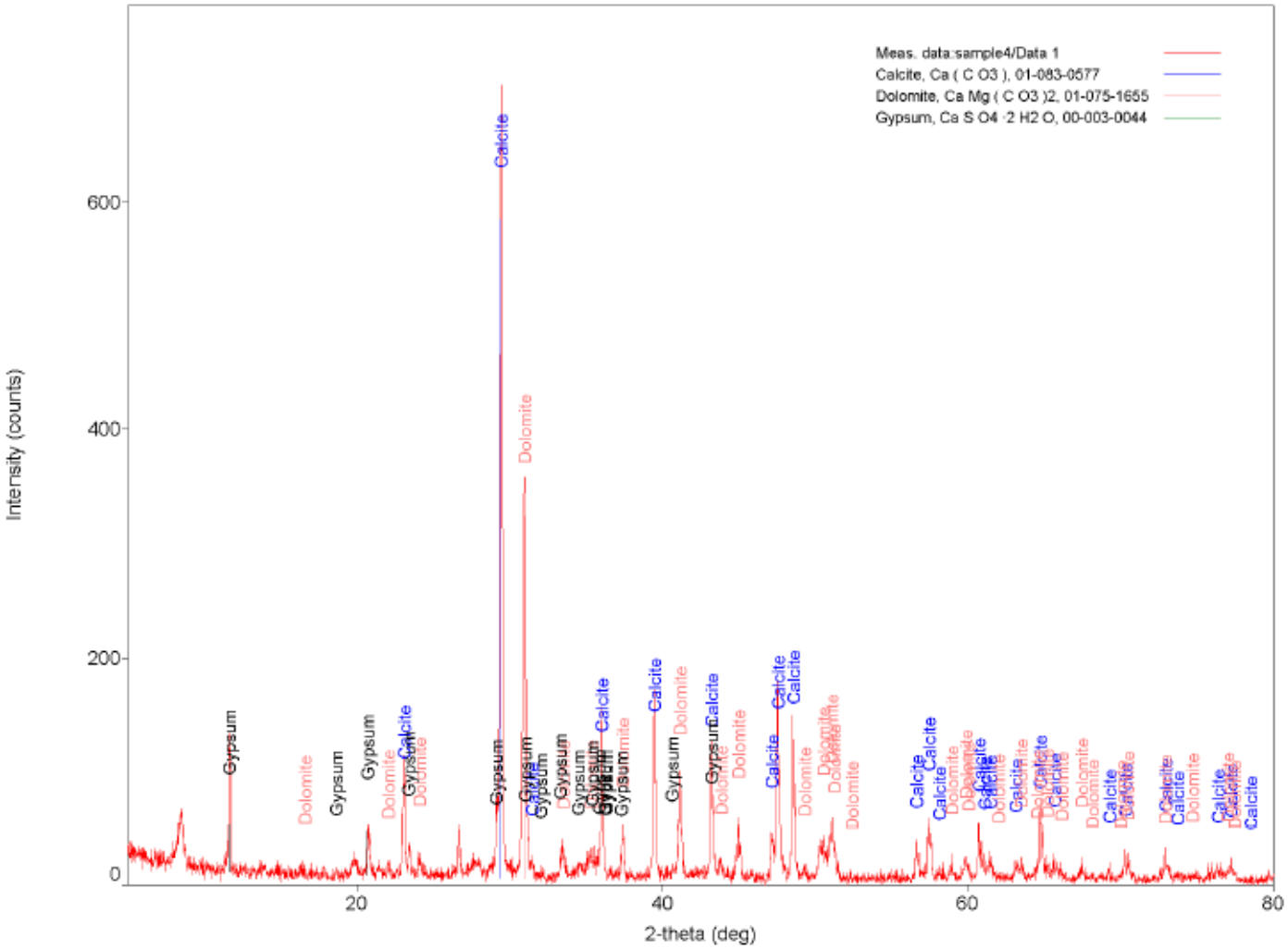

Figure B-4 XRD graph of sample (4)

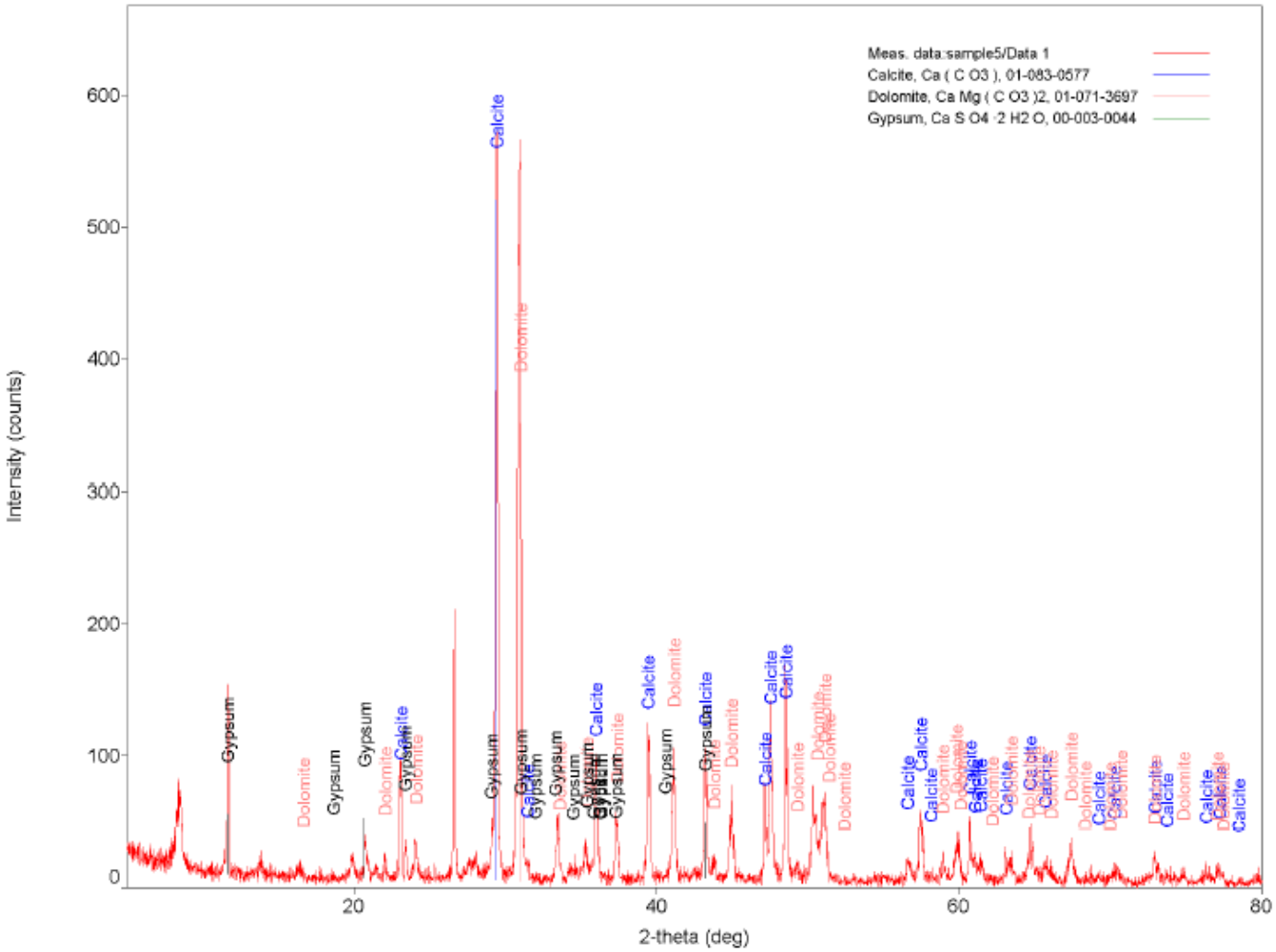

Figure B-5 XRD graph of sample (5)

Table B-1 results of XRF test for sample (1)

2014-12- 9 15:54

SQX Calculation Result

Sample : Sample1
Application : EZS001XNV Model : Bulk
Date analyzed : 2014-12- 9 15:40
Balance :
Matching library:
File : Hala1

No.	Component	Result	Unit	Det.limit	El.line	Intensity	w/o normal
1	F	0.281	wt%	0.09258	F -KA	0.0432	0.2104
2	Na2O	0.266	wt%	0.01487	Na-KA	0.9402	0.1991
3	MgO	18.6	wt%	0.01608	Mg-KA	175.0697	13.9432
4	Al2O3	3.32	wt%	0.00600	Al-KA	68.5626	2.4872
5	SiO2	18.4	wt%	0.01102	Si-KA	347.6974	13.7651
6	P2O5	0.0164	wt%	0.00173	P -KA	0.6563	0.0123
7	SO3	2.85	wt%	0.00337	S -KA	98.6707	2.1321
8	Cl	0.195	wt%	0.00382	Cl-KA	4.0076	0.1463
9	K2O	0.172	wt%	0.00253	K -KA	13.7760	0.1288
10	CaO	53.8	wt%	0.00975	Ca-KA	2736.1031	40.2917
11	TiO2	0.216	wt%	0.01579	Ti-KA	1.0345	0.1619
12	MnO	0.0406	wt%	0.00678	Mn-KA	0.9528	0.0304
13	Fe2O3	1.64	wt%	0.03857	Fe-KB1	10.8977	1.2250
14	CuO	0.0070	wt%	0.00315	Cu-KA	0.6574	0.0052
15	SrO	0.0556	wt%	0.00186	Sr-KA	24.7247	0.0416
16	ZrO2	0.0126	wt%	0.00207	Zr-KA	11.0911	0.0095
17	BaO	0.134	wt%	0.04742	Ba-LA	0.2878	0.1001

Table B-2 results of XRF test for sample (2)

2014-12- 9 16:09

SQX Calculation Result

Sample : Sample2
Application : EZS001XNV Model : Bulk
Date analyzed : 2014-12- 9 15:56
Balance :
Matching library:
File : Hala2

No.	Component	Result	Unit	Det.limit	El.line	Intensity	w/o normal
1	F	0.246	wt%	0.09942	F -KA	0.0390	0.1998
2	Na2O	0.343	wt%	0.01204	Na-KA	1.2525	0.2792
3	MgO	6.26	wt%	0.01121	Mg-KA	61.3103	5.0874
4	Al2O3	4.13	wt%	0.00613	Al-KA	102.8079	3.3542
5	SiO2	21.6	wt%	0.01107	Si-KA	485.6408	17.5409
6	P2O5	0.0307	wt%	0.00157	P -KA	1.4051	0.0250
7	SO3	0.678	wt%	0.00230	S -KA	26.8564	0.5510
8	Cl	0.201	wt%	0.00334	Cl-KA	4.8021	0.1637
9	K2O	0.163	wt%	0.00231	K -KA	14.9736	0.1324
10	CaO	63.6	wt%	0.01021	Ca-KA	3518.5802	51.7185
11	TiO2	0.288	wt%	0.01519	Ti-KA	1.3521	0.2339
12	V2O5	0.0320	wt%	0.01382	V -KA	0.2460	0.0260
13	MnO	0.0321	wt%	0.00656	Mn-KA	0.7358	0.0261
14	Fe2O3	2.22	wt%	0.03898	Fe-KB1	14.4275	1.8057
15	NiO	0.0112	wt%	0.00365	Ni-KA	0.7585	0.0091
16	SrO	0.0659	wt%	0.00183	Sr-KA	28.2445	0.0536
17	ZrO2	0.0042	wt%	0.00110	Zr-KA	8.7029	0.0034
18	BaO	0.0984	wt%	0.02668	Ba-KA	4.0456	0.0800

Table B-3 results of XRF test for sample (3)

2014-12- 9 16:56

SQX Calculation Result

Sample : Sample3
Application : EZS001XNV Model : Bulk
Date analyzed : 2014-12- 9 16:43
Balance :
Matching library:
File : Hala3

No.	Component	Result	Unit	Det.limit	El.line	Intensity	w/o normal
1	F	0.201	wt%	0.10238	F -KA	0.0339	0.1650
2	Na2O	0.644	wt%	0.01383	Na-KA	2.4969	0.5299
3	MgO	10.8	wt%	0.01350	Mg-KA	110.0503	8.8626
4	Al2O3	4.69	wt%	0.00660	Al-KA	114.4350	3.8577
5	SiO2	23.4	wt%	0.01182	Si-KA	510.3048	19.2806
6	P2O5	0.0606	wt%	0.00199	P -KA	2.6287	0.0499
7	SO3	6.34	wt%	0.00455	S -KA	235.4751	5.2120
8	Cl	0.798	wt%	0.00464	Cl-KA	16.9765	0.6566
9	K2O	0.393	wt%	0.00249	K -KA	32.1918	0.3230
10	CaO	49.3	wt%	0.00923	Ca-KA	2637.2224	40.5326
11	TiO2	0.335	wt%	0.01748	Ti-KA	1.8158	0.2757
12	Cr2O3	0.0445	wt%	0.00863	Cr-KA	0.6710	0.0366
13	MnO	0.0496	wt%	0.00589	Mn-KA	1.2760	0.0408
14	Fe2O3	2.37	wt%	0.03436	Fe-KB1	17.7605	1.9469
15	NiO	0.0111	wt%	0.00356	Ni-KA	0.8620	0.0091
16	ZnO	0.0098	wt%	0.00248	Zn-KA	1.3814	0.0081
17	SrO	0.403	wt%	0.00169	Sr-KA	197.4206	0.3311
18	ZrO2	0.0292	wt%	0.00960	Zr-KB1	3.5537	0.0240
19	BaO	0.120	wt%	0.02544	Ba-KA	5.4414	0.0984

Table B-4 results of XRF test for sample (4)

2014-12- 9 17:10

SQX Calculation Result

Sample : Sample4
Application : EZS001XNV Model : Bulk
Date analyzed : 2014-12- 9 16:57
Balance :
Matching library:
File : Hala4

No.	Component	Result	Unit	Det.limit	El.line	Intensity	w/o normal
1	F	0.232	wt%	0.09896	F -KA	0.0371	0.1875
2	Na2O	0.291	wt%	0.01382	Na-KA	1.0833	0.2348
3	MgO	9.41	wt%	0.01308	Mg-KA	92.5412	7.5912
4	Al2O3	3.87	wt%	0.00602	Al-KA	93.0032	3.1195
5	SiO2	19.1	wt%	0.01064	Si-KA	417.2740	15.4341
6	P2O5	0.0427	wt%	0.00162	P -KA	1.9327	0.0345
7	SO3	4.56	wt%	0.00382	S -KA	177.5247	3.6759
8	Cl	0.200	wt%	0.00345	Cl-KA	4.5335	0.1614
9	K2O	0.317	wt%	0.00245	K -KA	27.8127	0.2561
10	CaO	59.3	wt%	0.00989	Ca-KA	3201.7452	47.8361
11	TiO2	0.287	wt%	0.01883	Ti-KA	1.3893	0.2316
12	Cr2O3	0.0344	wt%	0.01003	Cr-KA	0.4623	0.0277
13	MnO	0.0551	wt%	0.00656	Mn-KA	1.3248	0.0445
14	Fe2O3	2.00	wt%	0.03670	Fe-KB1	13.3830	1.6108
15	NiO	0.0100	wt%	0.00374	Ni-KA	0.7010	0.0081
16	ZnO	0.0098	wt%	0.00263	Zn-KA	1.2462	0.0079
17	SrO	0.176	wt%	0.00181	Sr-KA	77.8171	0.1418
18	ZrO2	0.0147	wt%	0.00156	Zr-KA	24.7374	0.0118
19	BaO	0.103	wt%	0.02638	Ba-KA	4.3449	0.0833

Table B-5 results of XRF test for sample (5)

2014-12- 9 17:23

SQX Calculation Result

Sample : Sample5
Application : EZS001XNV Model : Bulk
Date analyzed : 2014-12- 9 17:10
Balance :
Matching library:
File : Hala5

No.	Component	Result	Unit	Det.limit	El.line	Intensity	w/o normal
1	F	0.265	wt%	0.10309	F -KA	0.0417	0.2111
2	Na2O	0.383	wt%	0.01421	Na-KA	1.3933	0.3057
3	MgO	11.1	wt%	0.01374	Mg-KA	108.2642	8.8809
4	Al2O3	3.60	wt%	0.00590	Al-KA	84.0548	2.8718
5	SiO2	17.9	wt%	0.01043	Si-KA	381.0439	14.2658
6	P2O5	0.0323	wt%	0.00145	P -KA	1.4471	0.0257
7	SO3	2.46	wt%	0.00299	S -KA	95.4924	1.9649
8	Cl	0.322	wt%	0.00378	Cl-KA	7.3785	0.2565
9	K2O	0.242	wt%	0.00240	K -KA	21.3654	0.1928
10	CaO	61.3	wt%	0.01022	Ca-KA	3302.5584	48.9103
11	TiO2	0.250	wt%	0.01909	Ti-KA	1.1758	0.1994
12	MnO	0.0513	wt%	0.00609	Mn-KA	1.1790	0.0409
13	Fe2O3	1.75	wt%	0.03729	Fe-KB1	11.3855	1.3924
14	SrO	0.187	wt%	0.00187	Sr-KA	80.9841	0.1492
15	BaO	0.140	wt%	0.02716	Ba-KA	5.7589	0.1117

APPENDIX C

CORRELATIONS TABLES OF MEASURED DATA

(METEOROLOFICAL DATA VS CONCENTRATIONS)

Table C-1 Correlations table of measured meteorological data and concentrations

Background Measurements

Construction Site Measurements (Receptor)	Temp. (^{o}C)	Humidity (%)	Pressure (HPasc)	Wind Speed (m/s)	Wind Direction (Degr.)	C_B (0-≤2.5) (µg/m^3)	C_B (>2.5-≤6) (µg/m^3)	C_B (>6-≤10) (µg/m^3)	C_B (>10-≤20) (µg/m^3)	C_B (>20-≤30) (µg/m^3)
Temp. (^{o}C)	0.99	-0.75	-0.14	0.31	-0.19	-0.23	-0.08	-0.03	-0.02	-0.32
Humidity (%)	-0.80	0.98	0.09	-0.41	-0.14	0.15	0.04	0.01	0.00	0.21
Pressure (HPasc)	-0.22	0.12	1.00	-0.04	0.20	0.05	0.00	0.00	-0.01	0.01
Wind Speed (m/s)	0.58	-0.43	-0.35	0.55	-0.13	-0.08	0.02	0.05	0.06	-0.03
Wind Direction (Degr.)	-0.01	-0.35	-0.01	0.44	0.60	0.19	0.11	0.08	0.07	0.08
C_R (0-≤2.5) (µg/m^3)	0.01	0.05	0.12	0.26	0.06	0.88	0.81	0.72	0.69	-0.06
C_R (>2.5-≤6) (µg/m^3)	0.02	-0.04	0.04	0.32	0.11	0.85	0.95	0.93	0.91	-0.05
C_R (>6-≤10) (µg/m^3)	0.05	-0.07	-0.02	0.35	0.10	0.73	0.95	0.97	0.97	-0.04
C_R (>10-≤20) (µg/m^3)	0.05	-0.06	-0.03	0.35	0.09	0.70	0.94	0.97	0.97	-0.04
C_R (>20-≤30) (µg/m^3)	0.05	-0.06	-0.04	0.34	0.08	0.65	0.91	0.96	0.97	-0.03

APPENDIX D

CORRELATIONS TABLES (METEOROLOGICAL DATA VS EMISSION RATES)

Table D-1 Correlation table of 15-minute averaged meteorological data and emission rates (wind sector 345-15^{o})

	Temp (^{o}C)	Humidity (%)	Pressure (HPasc)	Final Stability	Receptor Wind. Speed (m/s)	Receptor Wind Direct. (Degr.)	Background Wind Speed (m/s)	Background Wind Direct. (Degr.)
E`(0-2.5) (g/m^2.s)	-0.03	0.23	0.35	0.10	0.44	-0.29	0.49	0.01
E`(2.5-6) (g/m^2.s)	0.02	0.12	0.29	0.15	0.51	-0.13	0.48	-0.06
E`(6-10) (g/m^2.s)	0.34	-0.27	-0.19	0.21	0.76	0.16	0.64	-0.22
E`(10-20) (g/m^2.s)	-0.12	-0.13	-0.05	0.59	-0.09	0.03	-0.20	-0.14
E`(20-30) (g/m^2.s)	-0.21	-0.06	0.00	0.52	-0.31	0.01	-0.36	-0.06

Table D-2 Correlation table of 15-minute averaged meteorological data and emission rates (wind sector 15-45^{o})

	Temp (^{o}C)	Humidity (%)	Pressure (HPasc)	Final Stability	Receptor Wind. Speed (m/s)	Receptor Wind Direct. (Degr.)	Background Wind Speed (m/s)	Background Wind Direct. (Degr.)
E`(0-2.5) (g/m^2.s)	-0.34	0.65	0.45	0.00	0.53	0.22	0.52	-0.02
E`(2.5-6) (g/m^2.s)	-0.30	0.56	0.48	0.05	0.47	0.29	0.48	0.05
E`(6-10) (g/m^2.s)	-0.15	0.29	0.29	0.18	0.36	0.40	0.35	0.19
E`(10-20) (g/m^2.s)	-0.26	0.03	0.05	0.41	-0.38	0.28	-0.43	0.48
E`(20-30) (g/m^2.s)	-0.20	0.01	0.04	0.32	-0.34	0.24	-0.39	0.49

Table D-3 Correlation table of 15-minute averaged meteorological data and emission rates (wind sector 45-75^{o})

	Temp (^{o}C)	Humidity (%)	Pressure (HPasc)	Final Stability	Receptor Wind. Speed (m/s)	Receptor Wind Direct. (Degr.)	Background Wind Speed (m/s)	Background Wind Direct. (Degr.)
E`(0-2.5) (g/m^2.s)	0.13	-0.13	-0.07	0.12	0.36	0.09	0.28	-0.14
E`(2.5-6) (g/m^2.s)	0.09	-0.20	-0.21	0.23	0.16	0.17	0.11	-0.12
E`(6-10) (g/m^2.s)	0.11	-0.25	-0.31	0.27	0.11	0.17	0.07	-0.16
E`(10-20) (g/m^2.s)	-0.24	0.01	-0.37	0.38	-0.25	0.17	-0.29	-0.28
E`(20-30) (g/m^2.s)	-0.30	0.16	-0.30	0.29	-0.24	0.04	-0.30	-0.38

Table D-4 Correlation table of 15-minute averaged meteorological data and emission rates (wind sector 285-315^{o})

	Temp (^{o}C)	Humidity (%)	Pressure (HPasc)	Final Stability	Receptor Wind. Speed (m/s)	Receptor Wind Direct. (Degr.)	Background Wind Speed (m/s)	Background Wind Direct. (Degr.)
E`(0-2.5) (g/m^2.s)	-0.25	0.25	-0.50	0.39	0.42	0.04	0.43	0.16
E`(2.5-6) (g/m^2.s)	-0.03	-0.02	-0.57	0.43	0.70	0.15	0.61	0.19
E`(6-10) (g/m^2.s)	0.18	-0.24	-0.44	0.28	0.79	0.21	0.66	0.16
E`(10-20) (g/m^2.s)	-0.28	0.17	-0.08	0.61	-0.09	-0.28	-0.20	0.05
E`(20-30) (g/m^2.s)	-0.39	0.20	0.04	0.59	-0.36	-0.44	-0.44	0.00

Table D-5 Correlation table of <u>15-minute</u> averaged meteorological data and emission rates (wind sector 315-345^{o})

	Temp (^{o}C)	Humidity (%)	Pressure (HPasc)	Final Stability	Receptor Wind. Speed (m/s)	Receptor Wind Direct. (Degr.)	Background Wind Speed (m/s)	Background Wind Direct. (Degr.)
E`(0-2.5) (g/m^2.s)	-0.08	0.22	-0.04	0.27	0.32	0.21	-0.08	-0.21
E`(2.5-6) (g/m^2.s)	0.10	0.06	-0.11	0.15	0.58	0.27	0.01	-0.32
E`(6-10) (g/m^2.s)	0.21	-0.06	-0.19	0.04	0.68	0.30	0.05	-0.37
E`(10-20) (g/m^2.s)	0.05	0.04	-0.13	0.21	0.46	0.22	0.00	-0.24
E`(20-30) (g/m^2.s)	-0.09	-0.05	0.03	0.19	-0.13	-0.04	-0.08	0.04

Table D-6 Correlation table of <u>hourly</u> averaged meteorological data and emission rates (wind sector 15-45^{o})

	Temp (^{o}C)	Humidity (%)	Pressure (HPasc)	Final Stability	Receptor Wind. Speed (m/s)	Receptor Wind Direct. (Degr.)	Background Wind Speed (m/s)	Background Wind Direct. (Degr.)
E`(0-2.5) (g/m^2.s)	-0.96	0.97	0.62	0.07	0.72	0.24	0.88	-0.09
E`(2.5-6) (g/m^2.s)	-0.94	0.96	0.68	-0.02	0.70	0.28	0.87	-0.04
E`(6-10) (g/m^2.s)	-0.87	0.92	0.65	0.01	0.76	0.37	0.86	-0.01
E`(10-20) (g/m^2.s)	-0.79	0.85	0.42	0.26	0.87	0.33	0.84	-0.15
E`(20-30) (g/m^2.s)	-0.65	0.70	0.10	0.49	0.91	0.20	0.74	-0.31

Table D-7 Correlation table of <u>hourly</u> averaged meteorological data and emission rates (wind sector 45-75^{o})

	Temp (^{o}C)	Humidity (%)	Pressure (HPasc)	Final Stability	Receptor Wind. Speed (m/s)	Receptor Wind Direct. (Degr.)	Background Wind Speed (m/s)	Background Wind Direct. (Degr.)
E`(0-2.5) (g/m^2.s)	0.54	-0.41	0.09	-0.59	0.79	-0.27	0.73	-0.16
E`(2.5-6) (g/m^2.s)	0.73	-0.67	-0.08	-0.52	0.80	-0.15	0.80	-0.11
E`(6-10) (g/m^2.s)	0.82	-0.79	-0.35	-0.39	0.67	0.00	0.77	-0.06
E`(10-20) (g/m^2.s)	0.59	-0.68	-0.14	-0.17	0.34	0.13	0.46	0.31
E`(20-30) (g/m^2.s)	-0.55	0.27	0.52	0.49	-0.62	0.22	-0.58	0.51

Table D-8 Correlation table of <u>hourly</u> averaged meteorological data and emission rates (wind sector 285-315^{o})

	Temp (^{o}C)	Humidity (%)	Pressure (HPasc)	Final Stability	Receptor Wind. Speed (m/s)	Receptor Wind Direct. (Degr.)	Background Wind Speed (m/s)	Background Wind Direct. (Degr.)
E`(0-2.5) (g/m^2.s)	-0.67	0.82	-0.37	0.84	-0.54	0.44	0.19	-0.44
E`(2.5-6) (g/m^2.s)	-0.73	0.73	-0.50	0.90	-0.60	0.41	0.05	-0.46
E`(6-10) (g/m^2.s)	-0.56	0.83	-0.28	0.78	-0.42	0.55	0.28	-0.33
E`(10-20) (g/m^2.s)	-0.62	0.77	-0.37	0.84	-0.47	0.53	0.19	-0.34
E`(20-30) (g/m^2.s)	-0.87	-0.02	-0.99	0.89	-0.82	-0.12	-0.76	-0.53

Table D-9 Correlation table of <u>hourly</u> averaged meteorological data and emission rates (wind sector 315-345^{o})

	Temp (^{o}C)	Humidity (%)	Pressure (HPasc)	Final Stability	Receptor Wind. Speed (m/s)	Receptor Wind Direct. (Degr.)	Background Wind Speed (m/s)	Background Wind Direct. (Degr.)
E`(0-2.5) (g/m^2.s)	0.03	0.16	-0.09	0.18	0.55	0.31	-0.08	-0.30
E`(2.5-6) (g/m^2.s)	0.23	-0.06	-0.16	0.06	0.73	0.35	0.02	-0.39
E`(6-10) (g/m^2.s)	0.33	-0.18	-0.24	-0.01	0.79	0.39	0.05	-0.41
E`(10-20) (g/m^2.s)	0.28	-0.14	-0.22	0.05	0.76	0.36	0.04	-0.39
E`(20-30) (g/m^2.s)	-0.28	-0.05	0.10	0.26	-0.34	-0.11	-0.19	0.13